Earth-Science Reviews 243 (2023) 104483

Contents lists available at ScienceDirect

Earth-Science Reviews

journal homepage: www.elsevier.com/locate/earscirev

The global lead isotope system: Toward a new framework reflecting Earth's dynamic evolution

Luc S. Doucet [*,1], Zheng-Xiang Li [*,1], Denis Fougerouse, Hugo K.H. Olierook [2,3], Hamed Gamaleldien [1], Christopher L. Kirkland [2], Michael I.H. Hartnady [2]

School of Earth and Planetary Sciences, TIGeR, Curtin University, Perth, WA 6845, Australia

A R T I C L E I N F O

Keywords:
Lead
Isotopes
Mantle
U-Th-Pb

A B S T R A C T

The U-Th-Pb system is perhaps one of the most versatile isotopic systems in use by Earth scientists, widely applied to both date and compositionally trace geological events through Earth history. However, the Pb isotope systematics of the Earth are subject to two major paradoxes. Assuming our planet evolved uniformly from a chondritic composition, all the present-day Earth chemical reservoirs should plot on the 4.55 Ga meteorite isochron, also known as the *geochron;* but in fact, all known reservoirs are more radiogenic (having excess ^{206}Pb and ^{207}Pb) than the carbonaceous chondrites, constituting the first Pb paradox. The second Pb paradox (also called the kappa conundrum) is the apparent difference between the measured ^{232}Th/^{238}U ratio (κ) of oceanic basalts and the time-integrated ^{232}Th/^{238}U ratio (κ_{Pb}) predicted from the Pb isotope ratios. While significant progress has been made since the realization of the two Pb paradoxes over 50 years ago, the persistence of these issues highlights the limitations in our current understanding of the Earth's evolution with respect to U, Th and Pb, as we are neither able to ascertain the composition of the present-day bulk silicate Earth (BSE; comprising Earth's mantle and its crust) nor to determine the starting time(s) of U/Pb and Th/U fractionations in the mantle. In this contribution, we first review the Pb paradoxes and their proposed solutions. We then discuss the previously proposed Pb evolution models and establish a new framework based on a reassessment of global data and current understanding of Earth dynamics. Our model invokes the presence of distinct Pb isotope evolution paths for a diverse range of segregated components of the BSE, with the present-day upper continental crust being one of the end members. The model also features a two-stage Pb evolution for the silicate Earth, with a data-defined ca. 3.2 Ga start time for major compositional differentiation and remixing, possibly due to the initiation of global plate tectonics at that time. We readdress the first Pb paradox through recognizing that, to the first order, the Pb isotopic values of present-day Earth materials lie on a Pb differentiation line defined by our re-estimated present-day BSE and continental crust, and proposing that the data plot mostly to the right of the geochron due to second-order complications caused by both source mixing and fractionation of Earth materials. We argue that rocks found on Earth's surface mostly originated from more radiogenic reservoirs (with HIMU being an end member) at shallower levels, where long-term gravitational differentiation and subduction-led mantle remixing preferentially concentrated more radiogenic materials. We also largely mitigated the second Pb paradox through an updated κ vs. κ_{pb} plot using modern global databases, which shows a general agreement between the mean κ and κ_{pb} values. We further demonstrate that the choice of Pb evolution models has potentially profound implications when applying non-radiogenic Pb corrections during U-Pb dating of Earth materials.

1. Introduction

The U-Th-Pb system is perhaps one of the most versatile isotopic systems used by Earth scientists for both dating rocks and minerals and for compositionally tracing geological events through Earth's history (e.g. Bouvier and Wadhwa, 2010; Zindler and Hart, 1986). Thorium

* Corresponding authors.
E-mail addresses: luc-serge.doucet@curtin.edu.au (L.S. Doucet), z.li@curtin.edu.au (Z.-X. Li).
[1] Earth Dynamics Research Group.
[2] Timescales of Mineral Systems Group.
[3] John de Laeter Centre.

https://doi.org/10.1016/j.earscirev.2023.104483
Received 31 May 2023; Received in revised form 8 June 2023; Accepted 14 June 2023
Available online 23 June 2023

(^{232}Th) and the two radioactive isotopes of uranium (^{235}U and ^{238}U) decay into radiogenic Pb isotopes (^{208}Pb, ^{207}Pb and ^{206}Pb, respectively) with distinct half-lives (14 billion years or b.y., 700 million years or m.y. and 4.5 b.y., respectively), offering valuable temporal resolution that allows precise dating of rocks of all ages, using either the Pb-Pb isochrons or the U-Th-Pb method, or even the U-Th disequilibrium method for extremely young end dating.

Early pioneering work on isotopic systems focused on the determination of the age of our planet (Holmes, 1911; Holmes, 1913; Holmes, 1946; Holmes, 1947a; Holmes, 1947b; Houtermans, 1953). Such studies led to the first well-accepted approximation for Earth's age at 4.55 ± 0.07 billion years (Ga) by Claire Patterson (1956). Nowadays, in-situ U-Th-Pb geochronology via laser ablation inductively coupled (LA-ICPMS) or secondary ionization mass spectrometry (SIMS), alongside single-grain thermal ionization mass spectrometry (TIMS), is widely applied to address a broad range of questions in Earth Sciences (e.g., Schoene, 2014).

Whilst the U-Th-Pb system is the most used chronometer, it is also one of the most complex isotopic systems because U, Th, and Pb have distinct chemical behaviors. The two actinides, U and Th, are strongly lithophile and incompatible with rock-forming silicate minerals in Earth's mantle, preferring to be incorporated into Earth's crust. Also, U and Th tend to be concentrated in accessory minerals of low modal abundance (<1%), e.g., zircon, monazite, apatite, etc. The budget of U and Th is subject to the stability and behavior of those accessory minerals, which can be very complex (Bea and Montero, 1999; Hurley and Fairbairn, 1957; Pineda et al., 2022; Xiang et al., 2011). Lead is less incompatible than its parent isotopes. While also a lithophile, it has a strong chalcophile affinity. In addition, U and Pb are mobile in fluids, but only U with oxidation states of +6 is mobile, while +4 is immobile. Therefore, many geological processes can modify U/Pb, Th/Pb and U/Th ratios, and thus the U-Th-Pb isotopic systematics in Earth materials (Chauvel et al., 1995; Peucker-Ehrenbrink et al., 1994).

Assuming our planet evolved from a uniform chondritic composition, all the present-day Earth reservoirs should plot on the 4.55 Ga meteorite isochron, also known as the *geochron* (Murthy and Patterson, 1962) on a ^{207}Pb/^{204}Pb vs. ^{206}Pb/^{204}Pb diagram (Fig. 1a and Table 1). However, coined by Allègre (1968) as the *first Pb paradox*, the present-day mantle and the continental crust are more radiogenic (excess in ^{206}Pb and ^{207}Pb) than the carbonaceous chondrites and, on average, plot to the right of the geohron (Fig. 1b). The *second Pb paradox* (also called the *kappa conundrum* by Elliott et al. (1999)) was first coined by Tatsumoto (1966) and reiterated by Galer and O'Nions (1985). It refers to the difference between the measured ^{232}Th/^{238}U ratio (κ) in oceanic basalts and the time-integrated ^{232}Th/^{238}U ratio (κ_{Pb}) calculated from Pb isotope ratios (Fig. 2). In a chondritic-based closed system, the ^{208}Pb/^{206}Pb of a melt is a direct measure of ^{232}Th/^{238}U of its chondritic source, and κ_{Pb} and κ are expected to be of the same chondritic value. The conundrum is that oceanic rocks always have homogenous chondritic κ_{Pb} values (Blichert-Toft et al., 2010; Wipperfurth et al., 2018) suggesting a homogenous and chondritic mantle source, whereas the measured ^{232}Th/^{238}U (κ) shows a broad range, suggesting an open system.

For several decades, researchers sought solutions for these Pb paradoxes to better understand the crustal evolution of the Earth and its geochemical reservoirs (Fig. 3). While significant progress has been made, the persisting Pb paradoxes highlight limitations in our current understanding of the Earth's evolution, as we are neither able to ascertain the composition of the present-day bulk silicate Earth (BSE; comprising Earth's mantle and its crust) nor determine the starting time of U/Pb and Th/U fractionation of the mantle. In search for solution(s) to the Pb paradoxes, hundreds of articles have been published. In this contribution, we aim to summarize the generality of the key concepts in various proposed solutions for the Pb paradoxes, focusing mainly on the different previous Pb evolution models presented in seminal articles. Finally, based on those previous studies and a new assessment of global data, we attempt to propose a multi-dimensional framework for the Pb isotope evolution of both the BSE and its segregated components, with the present-day upper continental crust being one of the compositional end members.

2. Previously proposed solutions for the Pb paradoxes

Over the years, many researchers have attempted to find solutions to the Pb paradoxes. It is not the goal here to reiterate all those proposals; rather, we aim to summarize some of the most seminal works that have advanced our understanding of the topic (Fig. 3), so to provide a context for a refined Pb evolution model. For interested readers the present work will provide a useful starting point for the most relevant literature.

2.1. The first Pb paradox and its possible solutions

The seminal observation by Allègre (1968) that all Earth materials plot to the right of the geochron indicates that Earth has undergone significant U/Pb fractionation, and the so-called "accessible Earth" (i.e. oceanic basalts and continental crust) are sourced from high ^{238}U/^{204}Pb (μ) reservoirs relative to chondrite. This concept requires the existence of a complementary low-μ reservoir to balance the accessible Earth. The search for this *hidden* reservoir led to numerous studies, intending to identify this low-μ reservoir surmised to be located somewhere in

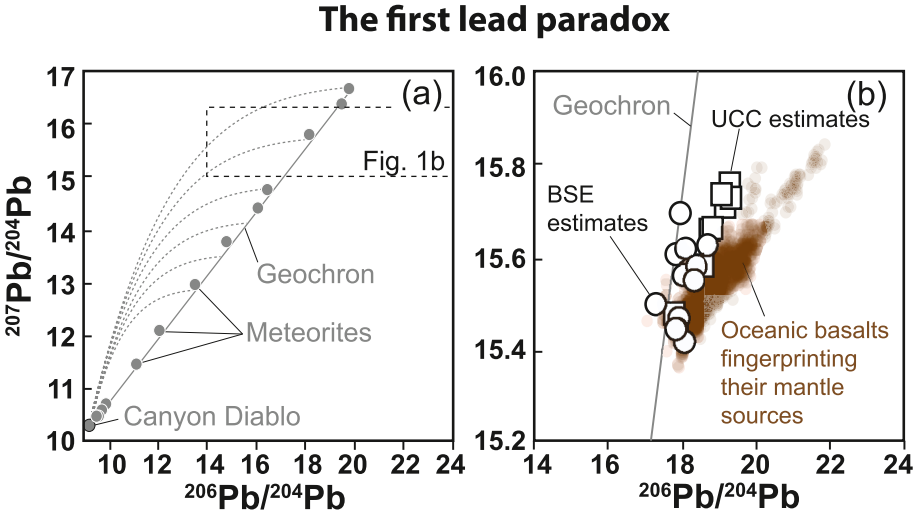

Fig. 1. The first Pb paradox. ^{206}Pb/^{204}Pb vs. ^{207}Pb/^{204}Pb for (a) meteorites 4.55 Ga isochrone, also known as the *geochron* (Murthy and Patterson, 1962), showing the locus of all Pb isotope compositions for different U/Pb ratios (the meteorite data can be found in Table 1), and (b) present-day oceanic igneous rocks (brown dots) fingerprinting the isotopic composition of the Earth's mantle (Supplementary Data Table 1) compared to Buk-Silicate Earth estimates (white circles; Table 2), upper continental crust (UCC) estimates (white squares; Table 2), and the *geochron*. If our planet evolved uniformly from a chondritic composition, the present-day Earth reservoirs should plot on the geochron, *but* the present-day mantle and the continental crust are more radiogenic (excess in ^{206}Pb and ^{207}Pb) and plot to the right of the geochron, constituting the first Pb paradox. (For interpretation of the references to colour in this figure legend, the reader is referred to the web version of this article.)

Table 1
Pb isotope compositions of meteorites used to establish the geochron.

NSample	Type		$^{206}Pb/^{204}Pb$	$^{207}Pb/^{204}Pb$	$^{208}Pb/^{204}Pb$	Reference
Canyon Diablo	IAB	Iron meteorite	9.307	10.294	29.476	Tatsumoto et al. (1973)
Mezo-Madaras	L3	Ordinary chondrite	9.589	10.459	29.731	Huey and Kohman (1973)
Abee	EH4	Enstatite chondrite	9.605	10.492	29.807	Huey and Kohman (1973)
Murchison	CM2	Carboniferous chondrite	9.666	10.499	29.699	Huey and Kohman (1973)
Murray	CM2	Carboniferous chondrite	9.806	10.594	29.939	Tatsumoto et al. (1973)
Odessa	IAB	Iron meteorite	9.995	10.691	30.087	Tatsumoto et al. (1973)
Allende	CV3	Chrondrite	11.233	11.466	31.458	Huey and Kohman (1973)
Allende	CV3	Chrondrite	11.25	11.451	31.352	Tatsumoto et al. (1973)
Beardsley	H5	Ordinary chondrite	12.193	12.106	31.973	Tatsumoto et al. (1973)
Plainview	H5	Ordinary chondrite	13.682	12.958	33.447	Tatsumoto et al. (1973)
Tennasilm	L4	Ordinary chondrite	15.012	13.753	35.237	Huey and Kohman (1973)
Paragould	LL5	Ordinary chondrite	16.309	14.422	36.094	Huey and Kohman (1973)
Plainview	H5	Ordinary chondrite	16.729	14.736	36.458	Huey and Kohman (1973)
Kunashek	L6	Ordinary chondrite	18.457	15.785	37.492	Huey and Kohman (1973)
Ladder Creek	L6	Ordinary chondrite	19.826	16.377	39.508	Huey and Kohman (1973)
Richardton	H5	Ordinary chondrite	20.123	16.656	39.853	Huey and Kohman (1973)

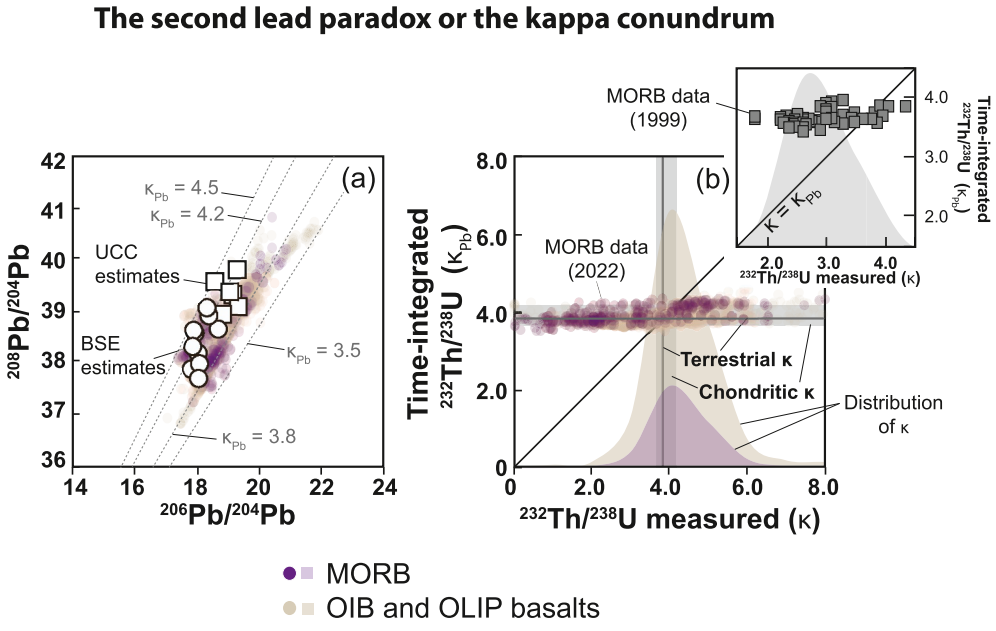

Fig. 2. The second Pb paradox (or the Kappa conundrum). $^{206}Pb/^{204}Pb$ vs. $^{208}Pb/^{204}Pb$ (a) and $^{232}Th/^{238}U$ (or κ) measured vs. time-integrated $^{232}Th/^{238}U$ (or κ_{Pb}) for present-day oceanic islands and oceanic plateau basalts (brown dots) and the mid-ocean ridge basalts (purple dots), fingerprinting the isotopic composition of the Earth's mantle. Inset in (b) shows the κ vs. κ_{Pb} MORB data available in 1999, featuring the discrepancy between κ and κ_{Pb} of mid-ocean ridge basalts, with κ mostly <4.0 and plotting to the left of the $\kappa = \kappa_{Pb}$ line whereas κ_{Pb} values plot close to the primordial (Blichert-Toft et al., 2010) and terrestrial κ (Wipperfurth et al., 2018). In (b) the distribution of κ based on our new compilation of present-day oceanic islands and oceanic plateau basalts (brown field) and the mid-ocean ridge basalts (purple field) shows that, overall, the present-day mantle has a chondritic κ (i.e., the peak of the approximately normal distributions agrees with the κ_{Pb} value). The scattering of the κ values is interpreted to reflect an open system in some of the analyzed samples or their sources. (For interpretation of the references to colour in this figure legend, the reader is referred to the web version of this article.)

Earth's interior.

2.1.1. Core Pb-pumping model

The effect of core formation on the U-Pb system has long been recognized (e.g., review by Ringwood, 1960), with both experimental work and theoretical modelling done to explain the discrepancy between the Pb composition of meteorite and that of Earth's mantle using the timing of core formation (Oversby and Ringwood, 1971; Vollmer, 1977). Allègre et al. (1982) revisited the influence of core formation on Pb isotope and coined the *core Pb-pumping model* (Fig. 3a), involving preferential incorporation of Pb into Earth's Fe-Ni core during and after core formation that increased the U/Pb ratio of the BSE (thus the higher radiogenic Pb content in present-day mantle and crust). Such a model requires a prolonged formation of Earth's core, i.e. up to >200 Ma after accretion to form the bulk of the core, followed by minor ongoing growth (Fig. 3a). Galer and Goldstein (1996) revisited the model of Allègre et al. (1982) by investigating the effect of accretion dynamics and core formation, and concluded that Pb-pumping occurred over a shorter time since Earth's accretion ($\geq 80 \pm 40$ Ma) with a relatively low bulk Earth μ (<4). The core Pb-pumping model requires a rather slow accretion, yet recent advances in the measurement of the Hf-W short-lived radioactive system on a range of meteorite samples suggest that core formation must have occurred rapidly, <75 to 120 Ma after accretion (Kleine et al., 2002; Rudge et al., 2010; Schoenberg et al., 2002; Thiemens et al., 2019; Yin et al., 2002). While such estimates remain controversial (Kruijer et al., 2021), most studies agree that a long-lived core growth (>200 Ma) was unlikely (Halliday and Canup, 2023). In the case of a rapid core formation, the role of the core in balancing the Pb isotopic composition of the present-day mantle and the crust becomes limited (Kamber and Kramers, 2006; Kramers and Tolstikhin, 1997; Murphy et al., 2003). Therefore, the existence of a hidden silicate reservoir has been invoked to balance the Pb isotopic composition of the present-day mantle and crust.

2.1.2. U/Pb fractionation in subduction zones

The chemical behavior of Pb differs markedly from U and Th, and it has been postulated by Chauvel et al., 1995 that during the subduction of oceanic crust/lithosphere, Pb will dissolve into fluids and be released

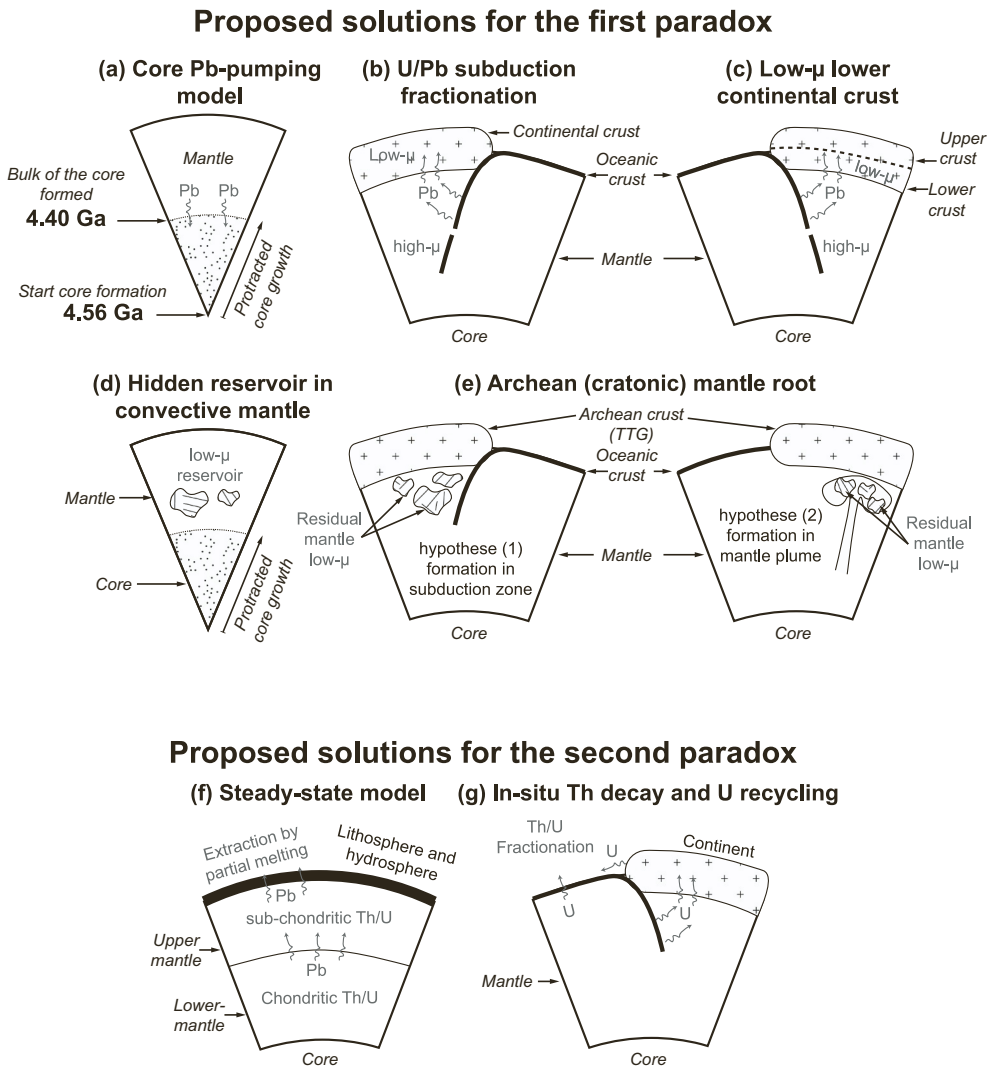

Fig. 3. Previously proposed solutions for the first and second Pb paradoxes. Solutions for the first paradox are summarized in (a) to (e), solutions for the second paradox are summarized in (f) and (g). (a) Core Pb-pumping model (Allègre et al., 1982), (b) U/Pb fractionation in subduction zones (Chauvel et al., 1995), (c) Low-μ store in the lower continental crust (Doe and Zartman, 1979; Zartman and Doe, 1981; Zartman and Haines, 1988), (d) hidden reservoir in the convective mantle (Burton et al., 2012; Malaviarachchi et al., 2008), (e) hidden reservoir in the cratonic mantle (Zhang et al., 2020) formed either in Archean subduction zones (hypothesis-1) or in Archean mantle plume (hypothesis-2) (Pearson et al., 2021), (f) the steady state model (Galer and O'Nions, 1985) and (g) the in-situ Th decay and U recycling solution (Allègre et al., 1986; Elliott et al., 1999; Tatsumoto, 1978).

into the mantle wedge, leaving the subducting slabs comparatively more enriched in U than Pb (i.e., high $^{238}U/^{204}Pb$, or HIMU) (Fig. 3b). Studies of obducted altered oceanic crust (e.g. Kelley et al., 2005; Niu, 2004) and altered serpentinite portions of oceanic slabs (Pettke et al., 2018) tend to support this model (Chauvel et al. (1995). In this model, Pb is preferentially released into the mantle wedge and may ultimately be incorporated into the continental crust during the formation of arc-type magmas, creating a low-μ reservoir in the crust, and complementary HIMU slabs that return to the mantle to be recycled into the source of oceanic basalts. The model of Chauvel et al. (1995) provides a robust explanation for the extreme radiogenic Pb isotope signatures ($^{206}Pb/^{204}Pb > 20$) of some ocean island basalts (Zindler and Hart, 1986), which fingerprint a HIMU source, interpreted to be derived from remelting of ancient oceanic slabs (Hofmann and White, 1982; Lassiter and Hauri, 1998). However, this model does not solve the first Pb paradox because the various estimates of the average isotopic composition of the accessible portion of the continental crust (i.e. the upper continental crust or UCC; a compilation of estimates are in Table 2, and are further discussed below in section 4.2) are more radiogenic than the mantle (including the HIMU) basalts and plot to the right of the geochron (Allègre and Lewin, 1989; Asmerom and Jacobsen, 1993; Davies, 1984; Kramers and Tolstikhin, 1997; Millot et al., 2004; Newsom et al., 1986; Othman et al., 1989; Zartman and Haines, 1988) (Fig. 1b).

2.1.3. *Low-μ lower continental crust*

In a series of papers, Doe and Zartman (1979), Zartman and Doe (1981) and Zartman and Haines (1988) developed the *plumbotectonics* model to account for the variability of Pb isotope signatures for different Earth reservoirs. These authors identified *mantle*, *upper crust*, *lower crust,* and *subcrustal lithosphere* (or continental lithospheric mantle) reservoirs. Their concept was to mimic the transport of elements (namely U, Th, and Pb) between different reservoirs during orogenic processes. One major modelling outcome of the various *plumbotectonic* models was the possible existence of a low-μ lower continental crust reservoir, plotting to the left of the geochron. Such models can therefore provide a process to balance the other reservoirs that plot to the right of the geochron. Kramers and Tolstikhin (1997) reached a similar conclusion using a *transport balance model*.

Having the lower crust as the hidden low-μ reservoir (Fig. 3c) presents an elegant solution for the first paradox, because this reservoir is not easily accessible, explaining *why* it was hidden for so long. Also, both geophysical and geochemical data suggest that the lower crust is depleted in U, Th, and K relative to the upper crust, and more mafic, it is therefore potentially enriched in Pb relative to U (Rudnick et al., 2003 and reference therein). However, Murphy et al. (2003), based on a compilation of crustal xenoliths, demonstrated that the average lower crust plots slightly to the right of the geochron, and concluded that it does not contain enough unradiogenic Pb to balance the other crustal reservoirs.

Table 2
Published Pb isotope compositions for the main Earth's reservoirs.

Name	Method	$^{206}Pb/^{204}Pb$	$^{207}Pb/^{204}Pb$	$^{208}Pb/^{204}Pb$	References
Bulk- Silicate Earth					
BSE_{SK75}-stage 1	Growth curve single stage	17.97	15.70	38.58	Stacey and Kramers (1975)
BSE_{SK75}-stage 2	Growth curve two stage	18.70	15.63	38.63	Stacey and Kramers (1975)
BSE_{CR75}	Growth curve single stage	17.84	15.61	37.88	Cumming and Richard (1975)
BSE_{MM20}	BSE mixing modeled	18.05	15.56	38.18	Maltese and Metzger (2020)
BSE_{GG91}	Total mass balance inversion	18.11	15.62	37.97	Galer and Goldstein (1991)
BSE_{ZD81}	Forward modelling - plumbotectonics model	18.08	15.42	37.68	Zartman and Doe (1981)
BSE_{M03}	Mass balance calculation	17.3	15.5		Murphy et al. (2003)
BSE_{L91}	Mass balance calculation	17.92	15.47	38.61	Liew et al. (1991)
BSE_{K89}	Evolution of carbonatites	17.882	15.445	38.317	Kwon et al. (1989)
BSE_{A88}	Mean composition of Tristant, Gough and Discovery	18.4	15.58	38.9	Allegre (1988)
BSE_{AL89}	Mean Ocean Island Basalts composition	18.34	15.551	39.05	Allegre and Lewin (1989)
BSE_{D84}	mean MORB	17.84	15.445		Davis (1984)
Upper mantle					
UM_{ZH88}	Forward modelling	18.47	15.48	37.73	Zartman and Haines (1988)
UM_{KT97}	Forward modelling	18.51	15.47	37.83	Kramers and Tolstikhin (1997)
Upper continental crust					
UCC_{KT97}	Forward modelling	19.17	15.71	39.32	Kramers and Tolstikhin (1997)
UCC_{AJ93}	Mean river sediments	19.30	15.76	39.8	Asmerom and Jacobsen (1993)
UCC_{ZH88}	Forward modelling - plumbotectonics model	19.33	15.73	39.07	Zartman and Haines (1988)
UCC_{N86}	Deep-sea sediments	18.76	15.66		Newsom et al. (1986)
UCC_{AL89}	Mass balance calculation	18.59	15.59	39.56	Allegre and Lewin (1989)
UCC_{D84}		17.80	15.48		Davis (1984)
UCC_{B89}	Mean oceanic floor sediments and Mn-nodules	18.84	15.67	38.923	Ben Othman et al. (1989)
UCC_{M04}	Mean river sediments	19.07	15.74	39.35	Millot et al. (2004)
Lower continental crust					
LC_{KT97}	Forward modelling	15.57	14.74	35.33	Kramers and Tolstikhin (1997)
LC_{RG90} (1)	Model based on lower crustal xenoliths	16.50	15.20		Rudnick and Golstein (1990)
LC_{RG90} (2)	Model based on lower crustal xenoliths	17.20	15.50		Rudnick and Golstein (1990)
LC_{ZH88}	Forward modelling - plumbotectonics model	17.62	15.35	38.75	Zartman and Haines (1988)
LC_{AJ93} (1)	Mass balance calculation	15.48	15.54	33.62	Asmerom and Jacobsen (1993)
LC_{AJ93} (2)	Mass balance calculation	18.59	15.47	36.53	Asmerom and Jacobsen (1993)
LC_{N86}	Mass balance calculation	15.96	15.30		Newsom et al. (1986)
Depleted MORB mantle					
DMM_{I87} (1)	Average all MORB	18.40	15.50	37.98	Ito et al. (1987)
DMM_{I87} (2)	Average N-MORB only	18.30	15.49	37.89	Ito et al. (1987)
DMM_{D84}	Most depleted MORB	17.34	15.40		Davis (1984)

2.1.4. Hidden reservoir in the convective mantle

Malaviarachchi et al. (2008) and Burton et al. (2012) reported unradiogenic Pb isotopic compositions that plot to the left of the geochron in bulk-rock residual portions of the Horoman massif (Japan) and in sulphides in abyssal peridotites, respectively. Both studies argued that these samples are fragments of a hidden low-μ reservoir that might represent a significant portion of the convective mantle and hence balance the Pb isotopic composition of Earth's accessible reservoir (Fig. 3d). Such a low-μ reservoir would also be the reservoir for unradiogenic osmium isotopic compositions found in the convective mantle, characterized by $^{187}Os/^{188}Os$ ratios lower than the estimate for the primitive upper mantle. The implication is that an ancient portion of the convective mantle contains relics of refractory mantle domains formed by ancient (<1.5 Ga) mantle melting events (e.g. Alard et al., 2005; Pearson et al., 2007). Mass balance calculations indicate that such a reservoir could balance the radiogenic isotopic composition of Earth's accessible material and perhaps solve the first Pb paradox. However, these mass balance calculations also require that a large portion of the convective mantle is unsampled, i.e., little such unradiogenic isotopic composition are sampled by mid-ocean ridge basalts, ocean island basalts, or oceanic plateau basalts. The significant lack of such unradiogenic Pb isotopes in these mantle-melt products would then constitute yet another paradox.

2.1.5. The Archean (cratonic) continental lithospheric mantle solution

Zhang et al. (2020) reported an unradiogenic Pb isotopic composition for a Cretaceous gabbro in the North China Craton that plotted to the left of the geochron. Those authors argued that the magma was produced by melting a low-μ cratonic mantle that was metasomatized during the Archean by subduction fluids enriched in unradiogenic Pb. In their model, Pb was trapped in sulphides at a shallow level (i.e., in the spinel stability field, <70 km) for billions of years before being released during cratonic destruction of the North China Craton during the Cretaceous. Overall, the highly refractory portion of the cratonic mantle appears to be a good candidate for a low-μ reservoir because it formed early in Earth's history, probably coeval with the extraction of the crust from the BSE (e.g. Pearson et al., 2007) (Fig. 3e). Given the behaviors of U and Pb, the cratonic lithosphere would develop a low-μ signature (and thereby low time-integrated $^{206}Pb/^{204}Pb$ and $^{207}Pb/^{204}Pb$). However, the concentration of both U and Pb, and the Pb isotopic composition, of the original cratonic mantle sample remains unknown because the intrinsically low concentration of both U and Pb makes cratonic peridotites very sensitive to post-melting processes where any higher concentration material could vastly dominate measured isotopic signatures (e.g., metasomatism and weathering; Boyd (1970); Boyd (1989)). A cratonic mantle has typically experienced complex pervasive metasomatic events (e.g. Pearson and Wittig, 2008), and trace elements are often overprinted during the transportation of mantle xenoliths from depth to the (near)surface (Doucet et al., 2013; Doucet et al., 2012). Finally, mantle xenoliths are generally intensively weathered, which may compromise the accuracy of their U-Th-Pb systematics. While the cratonic lithospheric mantle could potentially provide a solution as a hidden reservoir beneath continents, the lack of direct measurements inhibits definitive conclusions and calls for further investigation.

There are also other less mentioned models for the first Pb paradox. For example, Castillo (2015) explored the potential role of carbonate recycling in resolving the lead paradoxes, but the hypothesis remains largely untested. In fact, the hypothesis is not well supported by existing data (Castillo et al. (2018).

2.2. Previously proposed solutions for the second Pb paradox

The *second Pb paradox* (Galer and O'Nions, 1985; Tatsumoto, 1966) originally refers to the discrepancy between the measured $^{232}Th/^{238}U$ ratio (kappa or κ) in mid-oceanic ridge basalts (MORB) and time-integrated $^{232}Th/^{238}U$ ratio (kappa Pb or κ_{Pb}) (Fig. 2), with κ_{Pb} expressed as:

$$\kappa_{Pb(t)} = \frac{\left[\left(\frac{^{208}Pb}{^{204}Pb}\right)_t - \left(\frac{^{208}Pb}{^{204}Pb}\right)_{Primordial}\right]}{\left[\left(\frac{^{206}Pb}{^{204}Pb}\right)_t - \left(\frac{^{206}Pb}{^{204}Pb}\right)_{Primordial}\right]} \times \frac{\left(e^{\lambda^{238}U\times(4.56Ga-t)} - 1\right)}{\left(e^{\lambda^{232}Th\times(4.56Ga-t)} - 1\right)} \quad (1)$$

where $\lambda^{238}U$ and $\lambda^{232}Th$ are the decay constant of ^{238}U and ^{232}Th, 1.5512×10^{-11} yr^{-1} and 4.9475×10^{-11} yr^{-1} respectively (Jaffey et al., 1971; Le Roux and Glendenin, 1963). In a review of the second Pb paradox, Elliott et al. (1999) used geochemical data available at the time to show that MORB generally had $\kappa < \kappa_{Pb}$ (Fig. 2b inset). The κ_{Pb} of MORB is remarkably homogeneous at ~3.8 ± 0.2, similar to that of the chondrites, whereas the reported κ values of MORB range from 2.0 to 4.0 with an average value of ~2.5. To explain this discrepancy, Tatsumoto (1978), Galer and O'Nions (1985), Allègre et al. (1986), and Elliott et al. (1999) explored several mechanisms that could have caused the upper mantle, the source of MORB, to have low κ but chondritic κ_{Pb}. The first solution was the steady-state model of Galer and O'Nions (1985), featuring a stratified mantle (resulting from differentiation) consisting of a sub-chondritic ($\kappa << 3.8$) upper mantle and a chondritic lower mantle ($\kappa = 3.8$–4.0, depending on estimates at the time) (Fig. 3f). A second solution was a secular decrease of Th/U in the entire mantle (Allègre et al., 1986; Elliott et al., 1999; Tatsumoto, 1978) (Fig. 3g). This model is based on the change in fractionation factor between Th and U after the Great Oxidation Event due to preferential recycling of U in an oxidizing environment (Collerson and Kamber, 1999). According to this model, during the subduction of oceanic lithosphere, U dissolved by subduction fluids was released into the mantle wedge, leaving the subducting slabs comparatively more enriched in Th than U (high $^{232}Th/^{238}U$) and the mantle enriched in U relative to Th (low $^{232}Th/^{238}U$). Some of the uranium may ultimately be incorporated into the continental crust during the formation of arc-type magmas, then dissolved into fluids and released into the ocean before being recycled again into the mantle via subduction (Fig. 3g). Both processes decrease the mantle $^{232}Th/^{238}U$ ratio. Such a secular decrease in Th/U is observed through calculations of initial Th/U of zircon crystals from six kimberlites of varying ages (Zartman and Richardson, 2005) (Fig. 4). While the data from kimberlite zircons are scarce, they do show a decrease of κ between 2.5 Ga and the present-day, from 4.2–4.3 to 1.9–2.0.

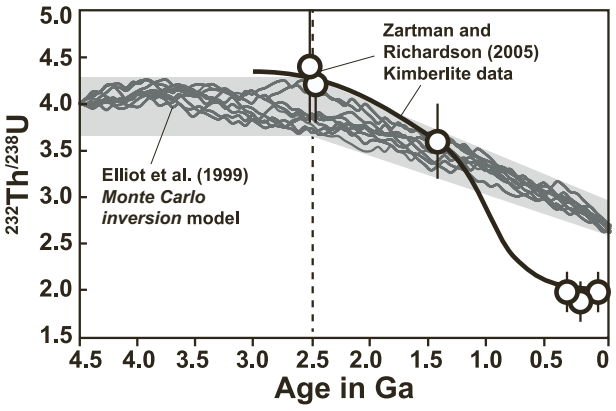

Fig. 4. Model for the secular evolution of Earth's mantle $^{232}Th/^{238}U$. The grey lines are from Elliott et al. (1999) and represent successful Monte Carlo inversions for secular evolution of κ. The white dots represent the composition of of melt in equilibrium with kimberlites (Zartman and Richardson, 2005).

Both models imply the existence of a homogeneous sub-chondritic mantle: the upper mantle in the steady-state model (Fig. 3f), and the entire mantle in the secular decrease model (Fig. 3g). These models were initially built upon a layered mantle assumption, but advances in global mantle tomography (e.g., Van der Hilst et al., 1997) and 4D geodynamic modelling (e.g., Zhong et al., 2007) have demonstrated the presence of a whole-mantle convective regime, therefore calling for a reevaluation. Wipperfurth et al. (2018) reported high precision $^{232}Th/^{238}U$ for unaltered mid-ocean ridge samples determined by laser ablation measurements (Arevalo and McDonough, 2010; Gale et al., 2013), along with a compilation of $^{232}Th/^{238}U$ data for ocean island basalts, and continental igneous, metamorphic and sedimentary rocks. They showed that overall, the Earth's mantle has chondritic $^{232}Th/^{238}U$ compositions. Our new compilation of oceanic basaltic data from the online global database Earthchem Portal (all data are available in Supplementary Data Table 1) shows that the mantle is far more heterogeneous than previously realized, with most samples having κ fall between 2 and 6 (Fig. 2b). Overall, 20% of ocean crust data (MORB and OIB) have $\kappa = \kappa_{Pb}$ (within ±0.2 of the analytical error), and the remainder fall on both sides of the κ_{Pb} values following a near-normal distribution, thus negating the need for a low-κ reservoir. We interpret the scattering of the κ values in comparison to the more consistent κ_{Pb} values as a result of a relatively open-system behavior of Th and U in some of the basaltic samples and/or their mantle sources in recent time (Andersen et al., 2015), whereas such processes did not significantly modify the $^{208}Pb/^{206}Pb$ ratio. Nonetheless, further work is needed to better examine and understand the cause(s) for individual cases where κ and κPb values diverge.

3. Existing framework for the Pb isotope system

3.1. Lead isotope growth curve models

Lead isotope growth curve models provide a way to constrain the temporal evolution of the Earth's main chemical reservoirs. The evolution of Pb isotopes can be formalized as:

$$\left(\frac{^{206}Pb}{^{204}Pb}\right)_{today} = \left(\frac{^{206}Pb}{^{204}Pb}\right)_{primordial} + \frac{^{238}U}{^{204}Pb} \times \left(e^{\lambda^{238}U\times t} - 1\right) \quad (2)$$

$$\left(\frac{^{207}Pb}{^{204}Pb}\right)_{today} = \left(\frac{^{207}Pb}{^{204}Pb}\right)_{primordial} + \frac{^{238}U}{^{204}Pb \times 137.818} \times \left(e^{\lambda^{235}U\times t} - 1\right) \quad (3)$$

$$\left(\frac{^{208}Pb}{^{204}Pb}\right)_{today} = \left(\frac{^{208}Pb}{^{204}Pb}\right)_{primordial} + \frac{^{232}Th}{^{204}Pb} \times \left(e^{\lambda^{235}U\times t} - 1\right) \quad (4)$$

with λ denoting the decay constants of U and Th (Jaffey et al., 1971; Le Roux and Glendenin, 1963) and $^{238}U/^{235}U = 137.818$ (Hiess et al., 2012).

From early on, researchers observed that the Pb isotope compositions of lead ore deposits, in the form of galena, appear to follow a simple isotopic growth curve (Cooper et al., 1969; Russell and Allan, 1955). Fig. 5 shows the growth distribution of the Pb isotope composition of Australian galena (Huston et al., 2019) (Supplementary Data Table 2). This observation led early workers to conclude that Earth's Pb isotopic composition could be approximated using various single-stage or multiple-stage Pb growth curves (Supplementary Data Table 3). It is important to realize that the assigned ages for the measured Pb isotopic ratios in galena deposits assumed the ages of the deposits to be the same as their 'conformable' host rock, i.e. volcanic-sedimentary ore deposits forming geologically stratiform lenses or layers with homogeneous Pb isotopic compositions. Whereas the age of host rocks could be determined using other methods (e.g., zircon U-Pb, with negligible common ^{204}Pb), the ages of the galena deposits could not be independently constrained. The Pb isotope signatures of these conformable Pb deposits

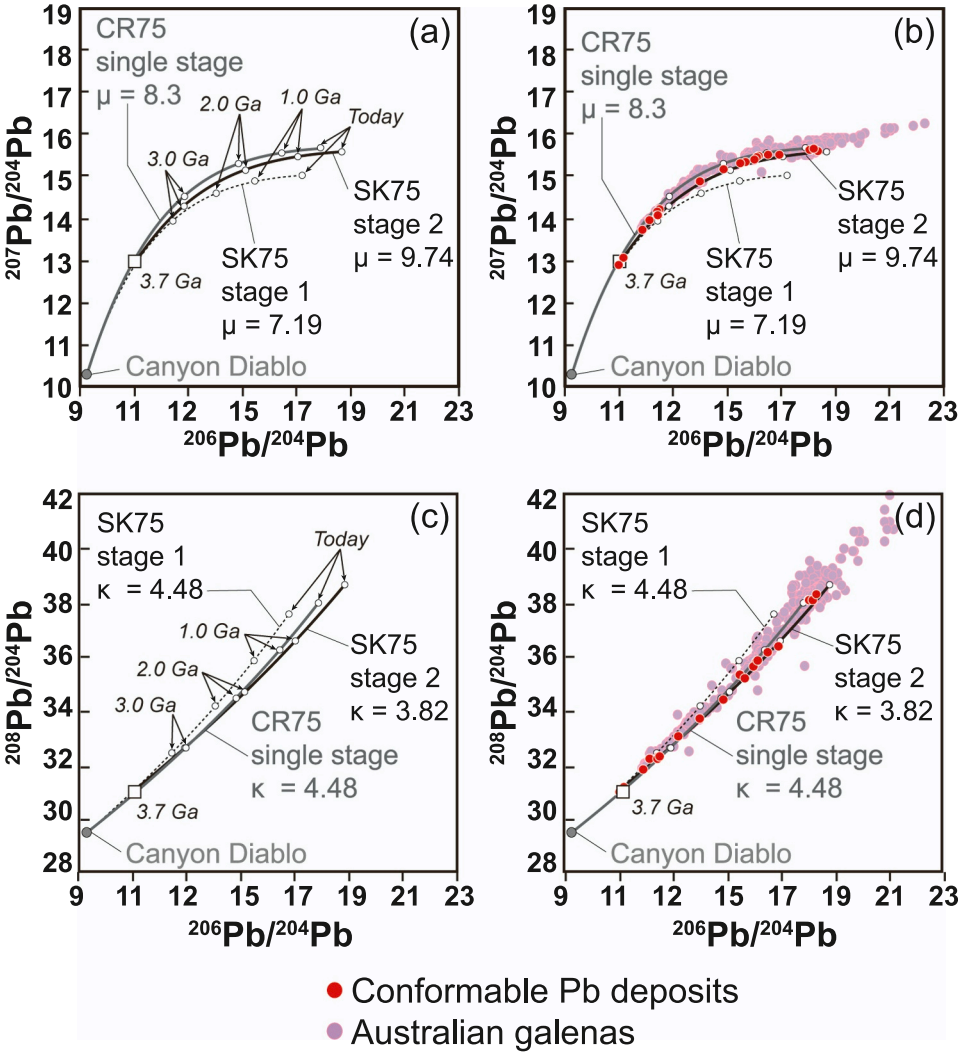

Fig. 5. Lead isotope evolution of Pb deposits. $^{206}Pb/^{204}Pb$ vs. $^{207}Pb/^{204}Pb$ (a and b) and $^{208}Pb/^{204}Pb$ (c and d) for conformable Pb deposits (red dots; see Table 3) and Australian Pb deposits (pink dots; data from Geoscience Australia (Huston et al. (2019) and Supplementary Data Table 2) compared with the single-stage Pb evolution model of Cumming and Richards (1975; CR75) and the two-stage model of Stacey and Kramers (1975; SK75). (For interpretation of the references to colour in this figure legend, the reader is referred to the web version of this article.)

were also believed to be intrinsically representative of their deep mantle sources rather than their surrounding country rocks (Russell et al., 1960; Stanton and Russell, 1959).

Based on the 'conformable' Pb concept (see detailed discussion in section 3.2 below), Russell and Allan (1955) and Cooper et al. (1969) established a list of conformable galena deposits (Table 3) that have been used by many subsequent studies to evaluate the evolution of Earth's Pb isotopic composition through time (e.g., Albarede and Martine, 1984; Cumming and Richards, 1975; Hartnady et al., 2022; Maltese and Mezger, 2020; Stacey and Kramers, 1975). The general approach involves combining Pb isotopic data from conformable Pb ore deposits and meteorites (Table 1) to yield the best fits of Pb isotopic data for the entire geological time (Stacey and Kramers, 1975). The additional general assumptions in those studies are that (1) the least radiogenic Pb material in the solar-system, troilite, extracted from the Canyon Diablo meteorite (Tatsumoto et al., 1973), represents the primordial composition for the Earth, and (2) the sources of the selected Pb ores evolved in either one or two stages and represent the Earth's composition at any given point in time (at the assumed ages of the deposits) since Earth's formation (Fig. 5). Such a Pb growth evolution is then used to constrain the ages of Pb ore deposits that have no other absolute age constraints, and such ages are called Pb-Pb model ages. The two-stage model of Stacey and Kramers, 1975 (shown as SK75 in Fig. 5) is a classic example of this that starts with stage 1 from 4.56 to 3.70 Ga, with initial $^{238}U/^{204}Pb$ and $^{232}Th/^{204}Pb$ ratios of 7.19 and 32.21, respectively (equivalent to initial $^{232}Th/^{238}U = 4.47$), and stage 2 from 3.7 Ga (age of oldest conformable Pb deposits) to present-day, with initial (at 3.7 Ga) $^{238}U/^{204}Pb$ and $^{232}Th/^{204}Pb$ ratios of 9.74 and 37.19, respectively ($^{232}Th/^{238}U = 3.8$). This two-stage model (Stacey and Kramers, 1975; Fig. 5) has been widely used for ore deposit studies, and importantly, also for correcting common Pb contamination in U-Pb dating (see section 6.1).

Albarede and Martine (1984) revisited the above concept and argued that "the analysis of the isotopic data on conformable ore bodies is hampered by the non-linear evolution of lead isotopic ratio with time…". They instead proposed a new method to linearize the growth curves by expressing the age component as the exponential of age multiplied by the radioactive decay constant (Fig. 6). Using this approach, the linear regressions can be expressed as:

$$\left(\frac{^{206}Pb}{^{204}Pb}\right)_t = -\frac{^{238}U}{^{204}Pb} \times e^{\left(\lambda^{238}U \times t\right)} + \left(\frac{^{206}Pb}{^{204}Pb}\right) \quad (5)$$

$$\left(\frac{^{207}Pb}{^{204}Pb}\right)_t = -\frac{^{235}U}{^{204}Pb} \times e^{\left(\lambda^{235}U \times t\right)} + \left(\frac{^{207}Pb}{^{204}Pb}\right) \quad (6)$$

$$\left(\frac{^{208}Pb}{^{204}Pb}\right)_t = -\frac{^{232}Th}{^{204}Pb} \times e^{\left(\lambda^{232}Th \times t\right)} + \left(\frac{^{208}Pb}{^{204}Pb}\right) \quad (7)$$

This approach confirmed that it is impossible to use a single-stage model to approximate Earth's Pb isotopic evolution because the linear regressions for the conformable Pb deposits do not intercept the Canyon

Table 3
Least radiogenic Pb isotope compositions of galena (PbS) from reference lead ore deposits.

NSample	Country	Type	Stratigraphic age	$^{206}Pb/^{204}Pb$	$^{207}Pb/^{204}Pb$	$^{208}Pb/^{204}Pb$	Reference	SK75 model ages			This study model ages		
			(Ma)					$t^{206}Pb$	$t^{207}Pb$	$t^{208}Pb$	$t^{206}Pb$	$t^{207}Pb$	$t^{208}Pb$
Halls Peaks	Australia	VMS?	285	18.35	15.607	38.347	Stacey and Kramer (1975)	214	379	153	360	891	334
Cobar	Australia	Vein style	410	18.082	15.624	38.125	Stacey and Kramer (1975)	384	815	273	520	788	441
Captain's Flat	Australia	Brine pool-type (Debated with SEDEX)	424	18.05	15.619	38.145	Stacey and Kramer (1975)	403	666	262	538	819	431
Bathurst	Canada	Brine pool-type (Debated with SEDEX)	460	18.204	15.655	38.122	Stacey and Kramer (1975)	307	4726	274	447	568	442
Balmat	USA	Shear zone hosted, remobilized SEDEX-MVT	1080	16.935	15.505	36.423	Stacey and Kramer (1975)	1062	769	1165	1162	1355	1245
Sullivan	Canada	SEDEX	1450	16.526	15.504	36.195	Cumming and Richards (1975)	1287	775	1282	1376	1358	1350
McArthur River	Australia	sediment-hosted massive sulfide - mixed mantle and crustal Pb source	1637	16.156	15.474	35.887	Cumming and Richards (1975)	1485	959	1438	1564	1462	1492
Mount Isa	Australia	SEDEX	1660	16.111	15.46	35.847	Stacey and Kramer (1975)	1509	1034	1459	1586	1507	1510
Broken Hill	Australia	SEDEX	1685	16.007	15.397	35.675	Stacey and Kramer (1975)	1563	1317	1545	1638	1687	1589
Southwest Finland	Finland	metarmorphic veins	1900	15.676	15.328	35.233	Cumming and Richards (1975)	1732	1558	1767	1800	1854	1789
Sudbury	USA	Impact	1900	15.489	15.303	35.338	Cumming and Richards (1975)	1826	1632	1714	1889	1909	1742
Cobalt	USA	SEDEX-like (basinal fluids/unconformity-associated)	2170	14.87	15.16	34.44	Stacey and Kramer (1975)	2128	1978	2158	2177	2173	2143
Geneva Lake	USA	Stratabound Sulphide Deposits (SEDEX?)	2600	14.002	14.87	33.716	Stacey and Kramer (1975)	2528	2446	2508	2561	2561	2462
Rosetta	South Africa	Complex, disseminated sulfide ores in porphyry bodie	3160	12.52	14.22	32.29	Maltese and Mezger (2020)	3159	3058	3182	3167	3107	3074
Daylight Mine	South Africa	Gold-quart veins	3200	12.43	14.16	32.21	Maltese and Mezger (2020)	3195	3099	3219	3202	3137	3335
Daylight Mine	South Africa	Gold-quart veins	3230	12.431	14.065	32.27	Cumming and Richards (1975)	3195	3162	3191	3202	3207	3303
French Bob's Barberton	South Africa	Gold-quart veins	3230	12.461	14.077	32.285	Stacey and Kramer (1975)	3183	3154	3184	3188	3198	3294
Big Stubby	Australia	fault-fill within Archaean ultrabasic rocks and metasediments	3329	12.14	13.96	32.23	Maltese and Mezger (2020)	3311	3227	3209	3336	3279	3324
Doolena Gap	Australia	VMS	3471	11.89	13.71	31.81	Maltese and Mezger (2020)	3409	3366	3403	3449	3431	3548
Isua-Pb539	Greenland	Vein-type galenas from within metasomatized tonalitic gneiss (porphyry?)	3741	11.18	13.05	31.13	Maltese and Mezger (2020)	3674	3649	3715	3760	3750	3905
Isua-460,000	Greenland	Vein-type galenas from within metasomatized tonalitic gneiss (porphyry?)	3807	11.02	12.89	30.99	Maltese and Mezger (2020)	3754	3732	3788	3828	3814	3978

t20xPb: model age using 206Pb, 207Pb and 208Pb following method of Albarède and Martin (1984).

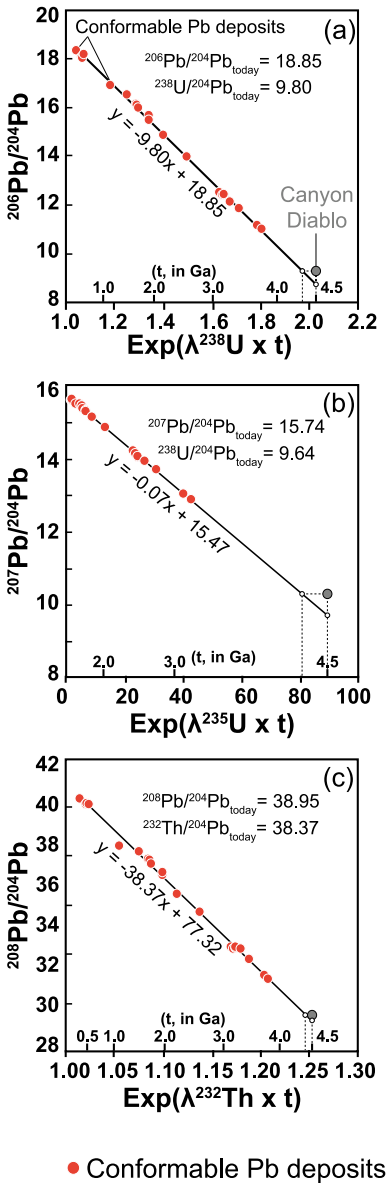

Fig. 6. Albarede and Martin (1984) linearization of Pb isotope composition of conformable Pb deposits. Age is expressed as a function of exp.(λt) vs. Pb $^{206}Pb/^{204}Pb$ (a), $^{207}Pb/^{204}Pb$ (b) and $^{208}Pb/^{204}Pb$ (c), with λ being the decay constants for ^{238}U, ^{235}U, and ^{232}Th (Jaffey et al., 1971; Le Roux and Glendenin, 1963). Note that the linear regression of the conformable Pb deposits does not intersect the Canyon Diablo, indicating some fractionation of U/Pb and Th/Pb after the formation of the Earth (Albarede, 2009; Hofmann, 2001).

Diablo composition (Fig. 6). The implication is that one or more continental differentiation events have likely taken place after Earth's formation, such as the 3.7 Ga event proposed by Stacey and Kramers (1975) and Hofmann (2001). This particular 3.7 Ga age coincides with the proposed time of high bolide impact flux on Earth and the Moon (the Late Heavy Bombardment; Harrison (2020)). Alternatively, an age of 3.7 Ga may reflect a time in Earth's history where the upper mantle irreversibly separated into the continental crust and depleted mantle components (Fisher and Vervoort, 2018). Evidence for this model stems from Hf isotopes in zircon, which reveal that there are virtually no suprachondritic Hf isotopic values prior to 3.85 Ga (Fisher and Vervoort, 2018); however, such small deviations in Hf space would be analytically challenging to resolve in the early Earth. In any case, this model implies that, before 3.85–3.80 Ga, the BSE was continually depleted and replenished as almost all continental crust-like materials were recycled back into the mantle. Only after 3.85–3.80 Ga did the continental crust segregate irreversibly from the mantle and the Pb isotopic composition of Earth's reservoirs fractionated into a depleted mantle and continental crust.

3.2. Sources of Pb in conformable Pb deposits and the evolution of the (ambiguous) "terrestrial lead"

As discussed above, Earth's Pb growth models, including that of Stacey and Kramers (1975), are constrained using conformable Pb deposits (Table 3) that have acted as a reference line that all Pb isotopic evolution models need to attempt to mimic/reproduce. However, the nature of the Pb reservoir tapped by the conformable Pb deposits remains ambiguous. Stacey and Kramers (1975) referred to their two-stage model as an "*approximation of terrestrial lead*", although at the time the nature of the reservoir was largely unknown. The term *terrestrial lead* has since been used by researchers to describe the Pb evolution of either the bulk-Earth, BSE, the mantle, or the continental crust. Hofmann (2001) challenged the use of conformable Pb deposits to describe the evolution of the mantle, or any primitive reservoir, by showing that recent galena deposits (including conformable deposits) have Pb isotope compositions close to that of oceanic and river sediments as well as to continental crust (Othman et al., 1989; Plank and Langmuir, 1998), but different from that of oceanic basalts (Fig. 7). Hofmann (2001) pointed out that marine and river sediments are enriched in Pb compared to oceanic basalts, and such enrichment results from continental contamination and, thus, the assumption made in previous studies that conformable Pb deposits were derived from the mantle "*cannot be correct*". On the other hand, we show in Fig. 7 that present-day oceanic volcanically-hosted massive sulphide deposits (VMS) formed along mid-ocean ridges (black smokers) plot close to mantle compositions (Andrieu et al., 1998; Fouquet and Marcoux, 1995; LeHuray et al., 1988; Verati et al., 1999). One would argue that these deposits have all the characteristics of conformable Pb deposits: they are stratiform and relatively homogeneous, and the deposits could track the isotopic composition of the mantle. However, it is important to note that oceanic VMS are not easily preserved in the geological record, and galena deposits (including conformable Pb deposits) are either VMS related to continental arc and rifting environments, sedimentary exhalative deposits (SEDEX, formed in continental rifting environments) or are epigenetic, stratabound deposits where mineralization occurred after host rock formation (Mississippi Valley-type; MVT) (Heinrich and Candela, 2014; Wilkinson, 2013; Table 3; Fig. 8). In all of the aforementioned Pb deposits (VMS, SEDEX, and MVT), it is accepted that Pb is leached by saline (10–30 wt% NaCl), moderate temperature (<250 °C) fluids, directly from the rocks in which these fluids percolate, whereas the contribution from magmatic fluids is relatively low (Robb (2013) and references therein). Therefore, the sources of Pb in VMS deposits formed along mid-ocean ridges are underlying MORBs, and the Pb for continental arc VMS, SEDEX and MVT deposits are sourced at least partially from continental crustal rocks. Conformable Pb deposits mostly represent (or are influenced by) the evolution of continental crust, and therefore should not be unconditionally used to infer the evolution of other reservoirs (such as bulk-Earth, BSE, or the mantle) (Hofmann, 2001; Leach et al., 2005; Richards, 1971).

3.3. Bulk Earth, Bulk Silicate Earth, and mantle estimates

All solutions proposed to solve the Pb paradoxes depend on a certain number of assumptions, such as the composition of the Bulk Earth, the present-day BSE, and the mantle. Estimating the composition of the Bulk Earth is the most challenging because of uncertainties caused by the giant impact Moon formation event (for details on the Moon impact, see Benz et al., 1989; Benz et al., 1986; Benz et al., 1987; Cameron, 1997; Cameron and Benz, 1991; Canup and Asphaug, 2001) and Pb lost from the Earth's mantle by volatilization during the giant impact and core

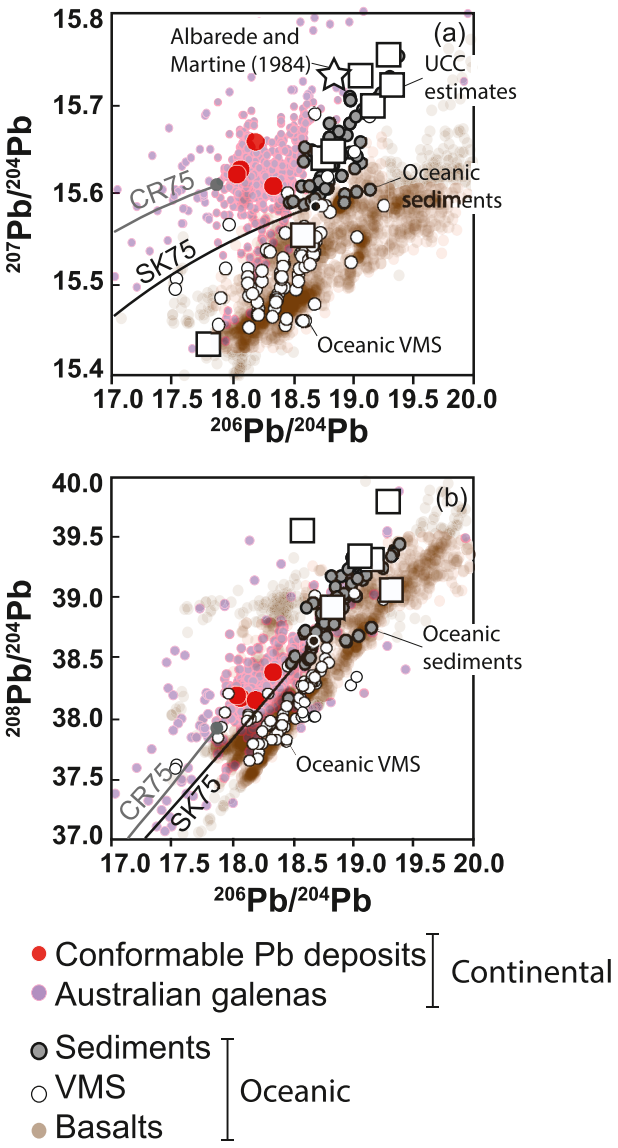

Fig. 7. Lead isotope composition of continental and oceanic Pb deposits. (a) $^{206}Pb/^{204}Pb$ vs. $^{207}Pb/^{204}Pb$ and (b) $^{206}Pb/^{204}Pb$ vs. $^{208}Pb/^{204}Pb$ plots of conformable Pb deposits (red dots; Table 3), Australian Pb deposits (pink dots; Supplementary Data Table 2), oceanic VMS (small white circles; Andrieu et al. (1998); Fouquet and Marcoux (1995); LeHuray et al. (1988); Verati et al. (1999)) and oceanic sediments (small grey circles;Plank (2014)) compared to estimates for the upper continental crust (white squares) (see Table 2) and present-day oceanic crust (brown dots). Note that oceanic VMS data plot in the same field as present-day oceanic crust while continental Pb deposits have excess in ^{207}Pb, like the upper continental crust. (For interpretation of the references to colour in this figure legend, the reader is referred to the web version of this article.)

formation (e.g. Connelly and Bizzarro, 2016; Halliday, 2004; Wood and Halliday, 2010). Nonetheless, the composition of at least sections of the present-day mantle can be indirectly measured in oceanic basalts, fingerprinting their mantle source (Dupré and Allègre, 1983; Hart, 1984; Kurz et al., 1982; Zindler and Hart, 1986).

There are currently over a dozen estimates for the Pb isotope composition of the BSE (Table 2), and those estimates can be categorized as being either *model-based* or *sample-based*. Model-based estimates use either forward modelling and/or mass balance calculations (see section 2), taking into account the timing of core differentiation and/or continental crust extraction (Galer and Goldstein, 1991; Liew et al., 1991; Maltese and Mezger, 2020; Murphy et al., 2003; Zartman and Doe,

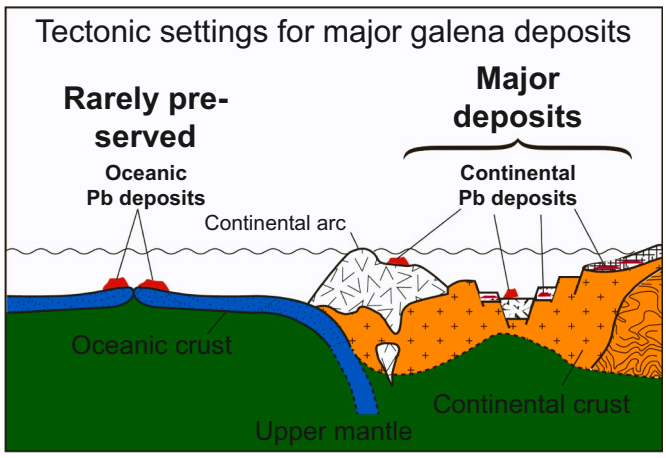

Fig. 8. Various tectonic settings for the formation of the major Pb deposits. There are three main Pb deposit types: (1) volcanogenic massive sulfide ore deposits (VMS) commonly associated with black smokers and oceanic spreading environments, (2) sedimentary exhalative ore deposits (SEDEX) and (3) Mississippi Valley-type ore deposits (MVT) (Andrieu et al., 1998; Fouquet and Marcoux, 1995; Heinrich and Candela, 2014; LeHuray et al., 1988; Verati et al., 1999; Wilkinson, 2013). It is beyond the scope of this contribution to explore the similarities and differences of these deposit types. VMS is the only type of deposit being formed in a mid-ocean ridge environment and thus fingerprint the Earth's upper mantle.

1981). Such estimates are intrinsically model-dependent because the exact timing of core formation or continental crust extraction remains debated. Another approach is to estimate the BSE using measured isotopic compositions of igneous rocks (Allègre and Lewin, 1989; Allègre et al., 1988; Davies, 1984; Kwon et al., 1989).

Before the emergence of global mantle tomography and 4D geodynamic modelling, some researchers argued, notably based on noble gas isotopic compositions of oceanic basalts, for a stratified mantle with an upper mantle depleted by extraction of the continental crust, and a lower mantle that would have retained its primitive, chondritic nature (Allègre et al., 1996; Allègre et al., 1983; White, 1985). In such a two-layer mantle convection model, ocean island basalts formed by mantle plumes rooted in the lower mantle can be used for fingerprinting the BSE (e.g. Allègre and Lewin, 1989; Allègre et al., 1988). Other researchers argued that the entire mantle had been depleted by differentiation processes and that the best estimates for BSE would therefore rely on samples that were least radiogenic (e.g. Davies, 1984). Modern studies show that, to the first-order, Earth's entire mantle is generally depleted relative to the BSE but also highly heterogeneous due to the recycling of surface material by subduction (Stracke, 2021 and reference therein), with subducted slabs going deep into the mantle, often all the way to the core-mantle boundary (Fukao and Obayashi, 2013; Goes et al., 2017; Shephard et al., 2017). However, while much of the mantle might have experienced various depletion and re-enrichment events, isotopic studies (He, Nd, W, Pb) of some deep-sourced plume-induced basalts show the existence of a primordial signature in their source aligned on the 4.50 Ga geochron, likely from the lower mantle (Jackson et al., 2020; Jackson and Carlson, 2011; Jackson et al., 2017; Wang et al., 2013) (Fig. 9).

4. A new framework for Pb isotopic growth models of dynamically evolving and heterogenous Earth reservoirs

4.1. A reappraisal of the BSE estimate

Because the composition of the Bulk Silicate Earth (BSE) is crucial for understanding the Pb isotopic evolution of the Earth, in this section, we propose a new BSE estimate based on a new compilation of mantle

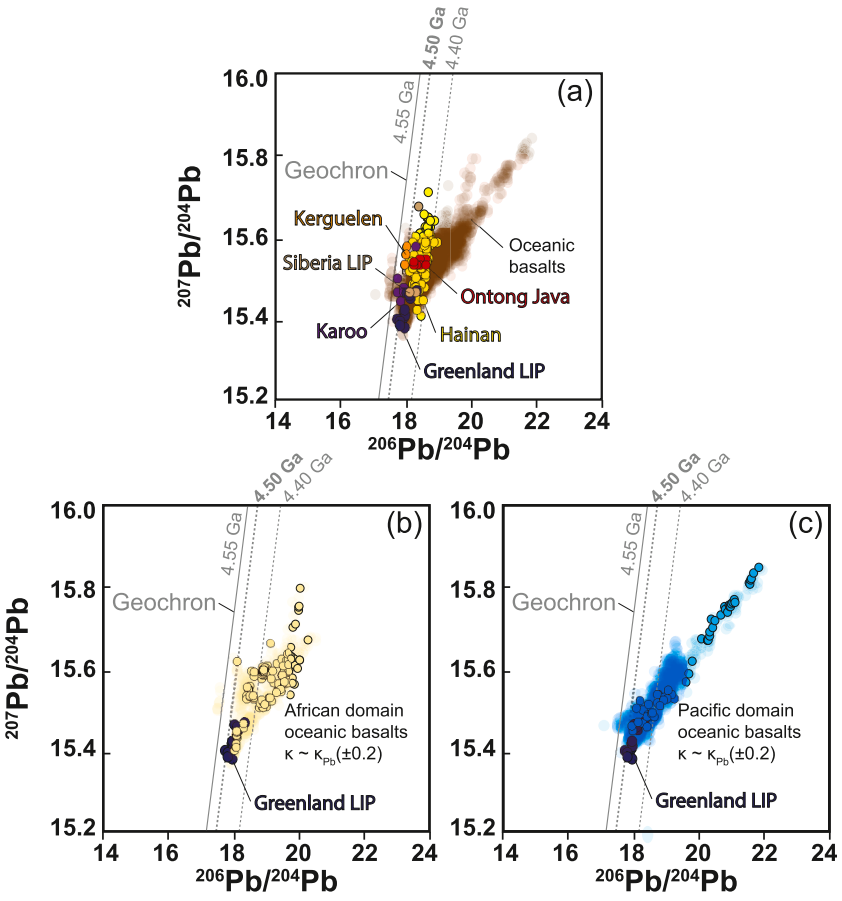

Fig. 9. (a) $^{206}Pb/^{204}Pb$ vs. $^{207}Pb/^{204}Pb$ plot of primitive materials from deep mantle plume sources, with data lying between the 4.55 and 4.40 Ga geochron (data sources: Jackson and Carlson, 2011; Jackson et al., 2010; Wang et al., 2013). Present-day global oceanic crust (OIB and MORB) is also shown as brown dots. (b and c) $^{206}Pb/^{204}Pb$ vs. $^{207}Pb/^{204}Pb$ plots of the African (b) and Pacific (c) mantle domain basalts (transparent dots) and samples with $\kappa \sim \kappa_{Pb} \pm 0.2$ (filled small black circles, with ±0.2 denoting the analytical uncertainties). (For interpretation of the references to colour in this figure legend, the reader is referred to the web version of this article.)

geochemical records coupled with new knowledge regarding mantle structure and global geodynamics discovered over the past decades.

If samples of BSE composition are preserved in the present-day mantle, they should plot close to the geochron. With respect to Pb, Earth has evolved as an essentially closed system since the Moon-forming impact that occurred between <75 to 120 Ma m.y. after initial accretion (Halliday and Canup, 2023). Therefore, the BSE should plot slightly to the right of the 4.56 Ga geochron, between the 4.50 and 4.46 Ga geochron on a $^{206}Pb/^{204}Pb$ vs. $^{207}Pb/^{204}Pb$ diagram, but should plot on 3.8–3.9 $^{232}Th/^{238}U$ lines on a $^{206}Pb/^{204}Pb$ vs. $^{208}Pb/^{204}Pb$ diagram (Blichert-Toft et al., 2010; Wipperfurth et al., 2018).

To define the present-day BSE composition, we evaluate the Pb isotopic results of worldwide oceanic basalts, including both MORB and oceanic intraplate volcanic rocks (Figs. 9 and 10). All the Pb isotope data used in this study are from the EarthChem Portal (www.earthchem.org), and precompiled datasets are available on GEOROC (http://georoc.mpch-mainz.gwdg.de/georoc/; data available in Supplementary Data Table 1 and Supplementary Data Fig. 1). Samples with mafic-intermediate affinities (SiO_2 = 40–55 wt%) were selected from the entire available datasets. The mantle sources of those rocks likely experienced complex histories of melt depletion, enrichment, and mixing (Willbold and Stracke, 2010). Their isotopic data, therefore, need to be filtered to eliminate the influence of such processes.

A series of recent studies showed that ocean island basalts and mid-ocean ridge basalts of the Pacific Ocean generally show significantly lower geochemical enrichment caused by subduction processes during the last supercontinent cycle, including the assembly and break-up of Gondwana and Pangea (Doucet et al., 2020b; Flament et al., 2022; Liu et al., 2021; Yang et al., 2021). As illustrated in Fig. 9b-c, African mantle domain basalts (oceanic basalts of mid-ocean ridge, ocean island, and oceanic plateau origins) are more radiogenic than that of the Pacific mantle domain, as evidenced by their positioning further away from the Geochron. The widely recognized mantle enrichment shown by African domain basalts has been attributed to the incorporation of recycled materials through subduction (Dupré and Allègre, 1983; Hart, 1984; Zindler and Hart, 1986). Therefore, for the analysis of BSE isotopic composition, we choose to use data from the Pacific mantle domain (oceanic basalts of mid-ocean ridge, ocean island, and oceanic plateau origins) that shows less enrichment by recycled sediments (Fig. 9b-c) (Doucet et al., 2020b; Flament et al., 2022; Liu et al., 2021; Yang et al., 2021).

We first filter the dataset by selecting samples with measured κ within uncertainty equal to that of the time-integrated κ_{Pb} calculated using Pb isotopes (measured $\kappa \sim \kappa_{Pb} \pm 0.2$, see Eq. 1). The filtered oceanic basalt compilation results in a well-defined $^{206}Pb/^{204}Pb$ vs. $^{207}Pb/^{204}Pb$ trend with $R^2 = 0.9$ (Fig. 10b), with an interception with the 4.50 Ga geochron close to the four least radiogenic samples which give mean values of $^{206}Pb/^{204}Pb = 17.84$ and $^{207}Pb/^{204}Pb = 15.44$, and fall onto the 4.50 Ga geochron. We use the $^{206}Pb/^{204}Pb$ and $^{207}Pb/^{204}Pb$ value of these least radiogenic sample to represent that of the BSE, which is close to the scattered primordial Pb isotope values identified from mantle plume-related basalts (Jackson et al., 2020; Jackson and Carlson, 2011; Jackson et al., 2017; Wang et al., 2013) (Figs. 9a and 10e-f). On the $^{206}Pb/^{204}Pb$ vs. $^{208}Pb/^{204}Pb$ diagram, the trend defined by the filtered samples (with $\kappa \sim \kappa_{Pb} \pm 0.2$) can be decomposed into a high-μ section ($^{206}Pb/^{204}Pb > 20$) characterized by $\kappa < 3.9$, characteristic of HIMU basalts (Elliott et al., 1999), and a normal-μ section ($^{206}Pb/^{204}Pb < 20$) with κ ranging from 3.8 to 4.2 (Fig. 10d, with filtered samples shown in filled black circles as in 10b). The least radiogenic sample have $^{208}Pb/^{204}Pb = 37.72$, with $\kappa = 3.9$, in line with values estimated using terrestrial samples (Blichert-Toft et al., 2010; Wipperfurth et al., 2018). Hence, our new BSE estimate is defined as $^{206}Pb/^{204}Pb = 17.84$,

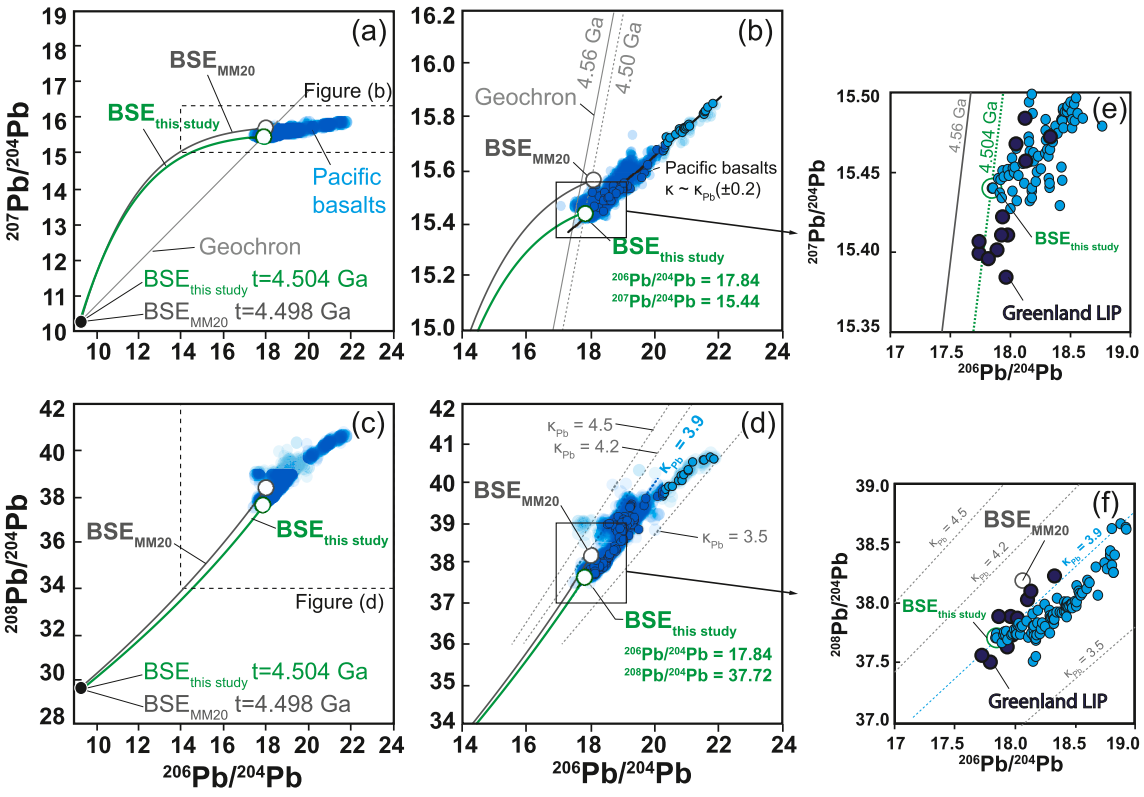

Fig. 10. Lead isotope evolution of the Bulk Silicate Earth. $^{206}Pb/^{204}Pb$ vs. $^{207}Pb/^{204}Pb$ (a, b and e) and $^{208}Pb/^{204}Pb$ (c, d and f) for Pacific basalts (blue dots). Samples with $\kappa \sim \kappa_{Pb} \pm 0.2$ (small black circles with blue fill, with ±0.2 denoting the analytical uncertainties) define a linear regression line in (b), expressed as: $\left(\frac{^{207}Pb}{^{204}Pb}\right) = 0.1064\ (\pm 0.0028) \times \left(\frac{^{206}Pb}{^{204}Pb}\right) + 13.518\ (\pm 0.055)$ with $R^2 = 0.9$. Samples that defines this regression come from Cook-Austral islands, Galapagos, Hawaii, Pitcairn, Society islands and East Pacific Rise (Supplementary Table 1). Also shown are the BSE growth curve from Maltese and Mezger (2020) (solid grey line) and the BSE growth curve from this study (solid green line) with $\mu = 8.41$, $\kappa = 3.9$ and present-day BSE with $^{206}Pb/^{204}Pb = 17.84$, $^{207}Pb/^{204}Pb = 15.44$ and $^{208}Pb/^{204}Pb = 37.72$. Also shown in (e) and (f) are samples from Greenland LIP (Jackson and Carlson, 2011; Jackson et al., 2010; Wang et al., 2013). (For interpretation of the references to colour in this figure legend, the reader is referred to the web version of this article.)

$^{207}Pb/^{204}Pb = 15.44$ and $^{208}Pb/^{204}Pb = 37.72$, similar to that based on the least radiogenic MORB (Davies, 1984). The four particular least radiogenic samples with almost identical $^{206}Pb/^{204}Pb$ and $^{207}Pb/^{204}Pb$ ratios came from Oahu Island, Hawaii (Roden et al., 1994; Tanaka et al., 2002).

It is important to note that most samples with unradiogenic Pb isotope values show suprachondritic Nd and Hf isotope signatures (εNd and εHf > 0) (Supplementary data Fig. 2), suggesting mantle sources that experienced depletion in incompatible elements through partial melt extraction if one accept the CHUR values as that of the BSE. However, whether such an assumption is correct remains a topic of ongoing debate (Boyet and Carlson, 2005; Burkhardt et al., 2016; Campbell and O'Neill, 2012; Caro et al., 2008; Dauphas, 2017; Frossard et al., 2022; Hasenstab-Dübeler et al., 2023; Sprung et al., 2013). If the BSE value we identified here is correct, it would imply that the Sm/Nd and Lu/Hf ratios of the BSE would be higher than the chondritic values (Supplementary data Fig. 2) as argued by some previous workers involving a variety of mechanisms.

4.2. Pb isotope composition of the continental crust

While about a dozen estimates exist for the Pb isotope composition of the continental crust (Table 2), the estimated value by Millot et al. (2004) has been the most accepted average isotopic composition for the accessible portion of the continental crust (i.e. the upper continental crust or UCC). Readers are referred to Millot et al. (2004) for details on their approach and calculations.

Millot et al. (2004) UCC Pb isotopic estimation was based on the Pb isotope composition of suspended sediments in Earth's major rivers (see Fig. 1 of Millot et al. (2004) for reference). The drainages of those major river systems cover a range of continental terranes, including both Archean terranes and younger orogens. Due to the large-scale integrating capacity of those river systems, suspended matters and sands have been considered representative of the average composition of the UCC. Millot et al. (2004) used two different and complementary calculations, the first of which was based on a flux-weighted average of particulate Pb delivered by the rivers, which gives 19.07, 15.74, and 39.35 for $^{206}Pb/^{204}Pb$, $^{207}Pb/^{204}Pb$, $^{208}Pb/^{204}Pb$, respectively. Their second estimate was based on the average value of each river system, which gives 18.93, 15.71, and 39.03, respectively. The first estimate has been the most widely used, however, in this study we explore both estimates for our revised Pb growth curve.

4.3. Exploring new Pb growth models

4.3.1. The BSE growth curves

4.3.1.1. Previous attempt for BSE growth curve. Maltese and Mezger (2020) revisited the Pb evolution of the Earth by considering Earth's accretion history on the U-Th-Pb system and derived a model for the evolution of the silicate Earth. The authors developed a method to estimate the initial composition of the BSE (hereafter BSE_{ini}) by considering the giant Moon-forming impact and subsequent core differentiation (Fig. 11). In that study, the authors modeled the impact between proto-Earth (volatile depleted and reduced) and the giant impactor known as Theia (volatile-rich and oxidized), the two major

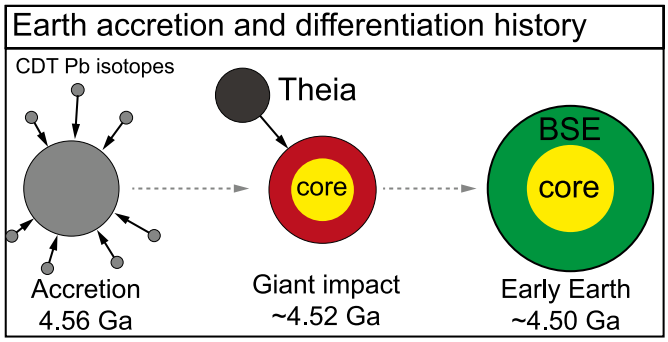

Fig. 11. Giant impact scenario and relative timings for the formation of Earth and the Moon. (a) Accretion of proto-Earth from chondrites with a Canyon Diablo Troilite (CDT) Pb isotopic composition. Proto-Earth started to differentiate just before (b) the collision with giant impactor Theia at ca. 4.52 Ga resulting in mixing and re-homogenization, followed by (c) the formation of BSE by rapid extraction of the core.

building blocks of Earth. The BSE composition can be reproduced by mixing 85% proto-Earth material with 15% Theia material. The mixing ratio was derived from the abundance of lithophile-refractory and moderately volatile elements in the BSE not affected by core formation, and is consistent with models for the giant impact process (for details on the Moon impact, see Benz et al., 1989; Benz et al., 1986; Benz et al., 1987; Cameron, 1997; Cameron and Benz, 1991; Canup and Asphaug, 2001). The proto-Earth formed through the accretion of highly volatile element-depleted materials with an extremely high μ (≥100) (O'neill, 1991a; O'Neill, 1991b), while Theia is assumed to have a CI chondritic composition (μ = 0.19) (Allegre et al., 1995; McDonough and Sun, 1995). Both bodies have chondritic $^{232}Th/^{238}U$ (Blichert-Toft et al., 2010; Wipperfurth et al., 2018), and the initial Pb isotopic composition of Canyon Diablo (Tatsumoto et al., 1973). A critical factor in this model is the time of mixing that can be deduced by re-constructing an evolution curve that matches the present-day BSE, making the Pb growth curve internally consistent. Maltese and Mezger (2020) used several BSE Pb isotopes estimates from the literature (see Table 2). Their preferred average solution yielded a time of impact of 69 ± 10 m.y. after accretion and initial Pb isotopic composition of the BSE of $^{206}Pb/^{204}Pb = 9.345$, $^{207}Pb/^{204}Pb = 10.37$ and $^{208}Pb/^{204}Pb = 29.51$, with associated BSE_{ini} μ = 8.63 and k = 4.05. It is important to note that those authors intentionally did not choose a specific BSE estimate and explored multiple solutions, and then critically explored the geological and geochemical meaning of the different results. As discussed above in section 3.3, defining a BSE estimate is critical and, in this study, we adopt the Maltese and Mezger (2020) approach to refine the BSE estimate and the Pb growth curves (see the section below).

4.3.1.2. New BSE growth curves. In this section, we follow the Maltese and Mezger (2020) approach to define the time of Proto-Earth–Theia impact and mixing, BSE_{ini} and BSE growth curve parameters (i.e., μ and k). Parameters for the mixing model can be found in Table 1 of Maltese and Mezger (2020), and the composition of present-day BSE has been defined in section 4.1 to be $^{206}Pb/^{204}Pb = 17.84$, $^{207}Pb/^{204}Pb = 15.44$ and $^{208}Pb/^{204}Pb = 39.48$. The Matlab code for the calculation is available in Research Data 1. The unique solution of BSE_{ini} based on our redefined present-day BSE Pb composition yields a time of impact of 56 ± 10 m.y. after Earth accretion with initial Pb isotope of the BSE being $^{206}Pb/^{204}Pb = 9.338$, $^{207}Pb/^{204}Pb = 10.36$ and $^{208}Pb/^{204}Pb = 29.50$, μ = 8.41 and k = 3.9. Measurement of the Hf-W short-lived radioactive system on a range of meteorites samples suggests a rapid core formation that must have occurred within <75–120 m.y. of accretion (Halliday and Canup, 2023), consistent with the time of mixing for the new BSE estimate. The above parameters of our new BSE estimate are close to those of Maltese and Mezger (2020), and lead to an internally consistent BSE Pb growth curve (Fig. 10) that can be defined as:

$$\left(\frac{^{206}Pb}{^{204}Pb}\right)_{BSE\ today} = 9.338 + 8.41 \times \left(e^{(\lambda^{238}U\times 4.504Ga)} - e^{(\lambda^{238}U\times t)}\right) \quad (8)$$

$$\left(\frac{^{207}Pb}{^{204}Pb}\right)_{BSE\ today} = 10.36 + \frac{8.41}{137.818} \times \left(e^{(\lambda^{235}U\times 4.504Ga)} - e^{(\lambda^{235}U\times t)}\right) \quad (9)$$

$$\left(\frac{Pb_{208}}{Pb_{204}}\right)_{BSE\ today} = 29.50 + (8.41 \times 3.9) \times \left(e^{(\lambda Th_{232}\times 4.504Ga)} - e^{(\lambda Th_{232}\times t)}\right) \quad (10)$$

4.3.2. The BSE growth curve and a redefined UCC growth curve vs. curves defined by conformable galena deposits

A striking feature of the new BSE growth model is that it agrees with the evolution curves defined by the Eo- and Paleo-Archean conformable Pb ore deposits (dated between 3.8 and 3.2 Ga) (Maltese and Mezger, 2020) (Table 3 and Figs. 11 and 12), and yields Pb-Pb model ages with uncertainties of ±20–30 Ma, in agreement with stratigraphic ages constrained via independent means (Table 3). On the other hand, Pb ore deposits younger than 3.2 Ga are systematically more radiogenic than the BSE growth curve (Figs. 12 and 13). This observation implies that no significant U/Pb and Th/U fractionation occurred in the source of Pb deposits before 3.2 Ga, i.e., the >3.2 Ga deposits exhibit a predominantly mantle signature (Maltese and Mezger, 2020). A regression line between the present-day UCC and BSE intersects the revised BSE Pb isotopic growth curve at 3.2 Ga (Fig. 12a), providing further evidence that a major extraction of continental crust from the BSE occurred at ~3.2 Ga (Millot et al., 2004) as suggested by global compilation for oxygen and hafnium isotopes in zircons (Kirkland et al., 2021; Wang et al., 2022). Based on this observation, we can define a continent growth model by connecting the 3.2 Ga BSE with the present-day UCC (Fig. 12). The preferred upper continental crust (UCC) growth model is defined by:

$$\left(\frac{^{206}Pb}{^{204}Pb}\right)_{UCC\ today} = \left(\frac{^{206}Pb}{^{204}Pb}\right)_{BSE\ at\ 3.2Ga} + 10.104 \times \left(e^{(\lambda^{238}U\times 3.2Ga)} - e^{(\lambda^{238}U\times t)}\right) \quad (11)$$

$$\left(\frac{^{207}Pb}{^{204}Pb}\right)_{UCC\ today} = \left(\frac{^{207}Pb}{^{204}Pb}\right)_{BSE\ at\ 3.2Ga} + \frac{10.104}{137.818} \times \left(e^{(\lambda^{235}U\times 3.2Ga)} - e^{(\lambda^{235}U\times t)}\right) \quad (12)$$

$$\left(\frac{^{208}Pb}{^{204}Pb}\right)_{CC\ today} = \left(\frac{^{208}Pb}{^{204}Pb}\right)_{BSE\ at\ 3.2Ga} + (10.329 \times 4.059) \times \left(e^{(\lambda^{232}Th\times 3.2Ga)} - e^{(\lambda^{232}Th\times t)}\right) \quad (13)$$

Using present-day UCC estimates from average basin values of Millot et al. (2004) ($^{206}Pb/^{204}Pb = 18.93$, $^{207}Pb/^{204}Pb = 15.71$ and $^{208}Pb/^{204}Pb = 39.03$), this growth model yields Pb-Pb model ages estimates closer to stratigraphic ages than other growth curve models (including Stacey and Kramers, 1975; =Table 3).

The newly defined continental Pb growth model (Figs. 12 and 13)

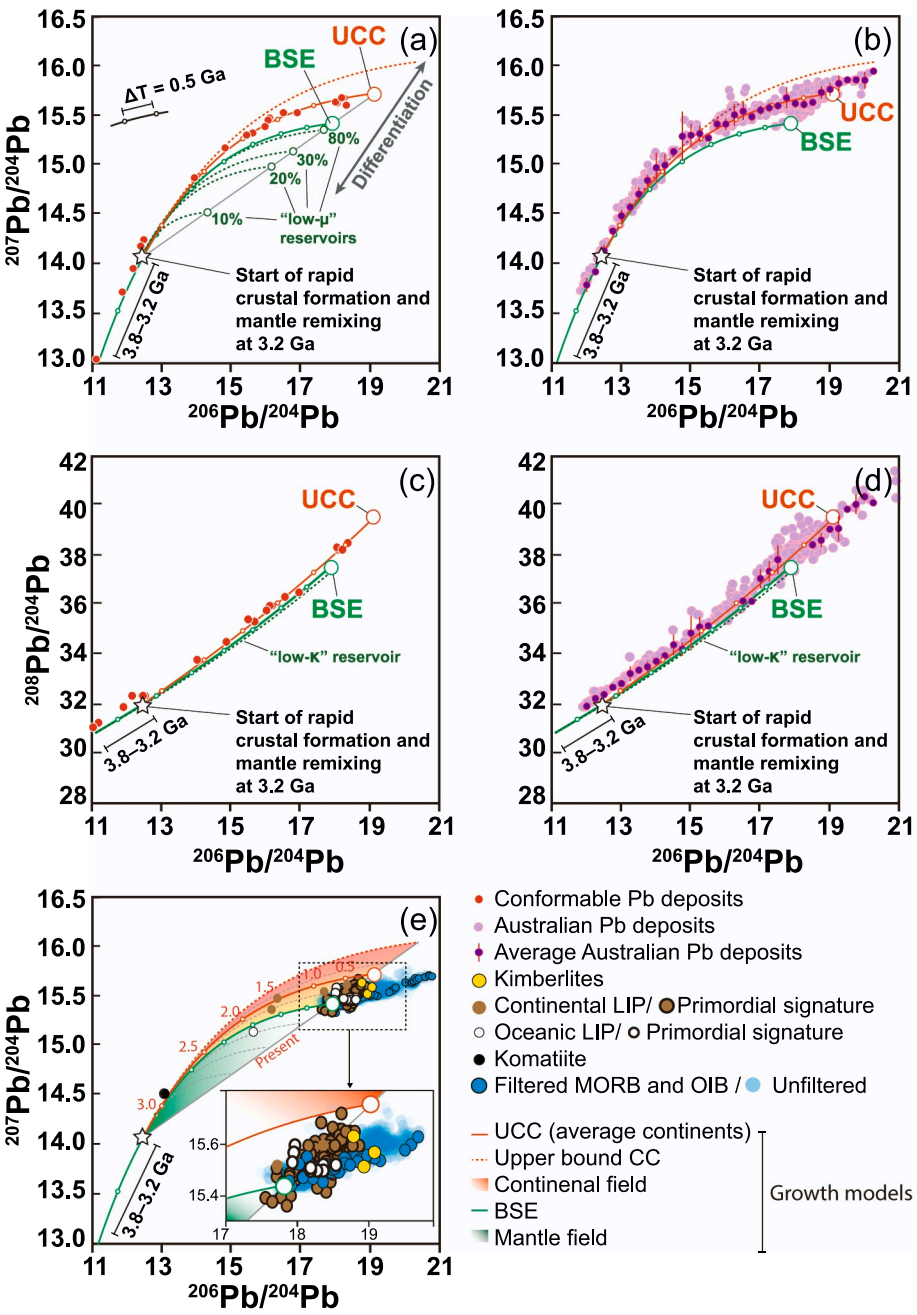

Fig. 12. Lead isotope growth curves for the Bulk Silicate Earth, the continental crust, and complementary mantle reservoirs. (a, b) $^{206}Pb/^{204}Pb$ vs. $^{207}Pb/^{204}Pb$ plots, (c, d) $^{206}Pb/^{204}Pb$ vs. $^{208}Pb/^{204}Pb$ plots, and (e) $^{206}Pb/^{204}Pb$ vs. $^{207}Pb/^{204}Pb$ diagram representing the range for possible Pb growth evolution for both the mantle and the continental crust after the start of rapid crustal formation and mantle remixing at 3.2 Ga. Pb isotope growth curves shown include that for the Bulk Silicate Earth (solid green line), for the average continental crust (solid orange line), for a speculated end member of the upper continental crust (dashed orange line; see data constraints in (b) and in Figs. 14b and 15), and for hypothesized notional complementary mantle reservoirs (dashed green lines). The average continental crust model starts at 3.2 Ga and is defined by $\mu = 10.3$ and $\kappa = 4.2$ (solid orange line, this study) to fit the upper continental crust (UCC; $^{206}Pb/^{204}Pb = 19.07$ $^{207}Pb/^{204}Pb = 15.74$ and $^{208}Pb/^{204}Pb = 39.35$; Millot et al. (2004), Table 6). Mass balance calculations predict that the complementary mantle reservoirs have low-μ and low-κ depending on the proportion of the mantle affected by continental extraction (10%, 20%, 30%, and 80% of continental extraction are shown for reference; see Method). The conformable Pb ore deposits (red dots) data in (a) and (c) are from (Cumming and Richards, 1975; Maltese and Mezger, 2020; Stacey and Kramers, 1975). The compilation of Australian Pb ore data (light purple dots) in (b) and (d) are from Geoscience Australia (Huston et al., 2019). The average evolution for the Australian Pb ore data (dark purple dots) were calculated using a bin of 0.25 $^{206}Pb/^{204}Pb$. (For interpretation of the references to colour in this figure legend, the reader is referred to the web version of this article.)

matches the evolution curves defined by the post-3.2 Ga conformable Pb ore deposits (dated between 2.6 and 0.24 Ga) (Cumming and Richards, 1975; Stacey and Kramers, 1975), that also approximates the average composition of Australian Pb ore deposits (Fig. 12b, c). The redefined BSE and continental growth models thus best explain the Pb ore deposits' evolution from 3.8 Ga to today by utilizing two distinct stages involving different sources: the mantle before 3.2 Ga, and predominantly the continental crust after 3.2 Ga.

4.3.3. *Pb isotope signatures of varying mantle-derived igneous rocks: Evidence for a heterogeneous mantle with a diverse range of reservoirs*

We now use the redefined BSE and continental crust Pb evolution curves as a guide to examine the Pb isotope characteristics of various mantle-derived igneous rocks.

At the time of melting, mantle-derived rocks have the same Pb isotopic compositions as their source but different U/Pb and U/Th. Thus, for ancient melt products, the initial Pb isotope composition needs to be corrected for the ingrowth of any excess radiogenic Pb since the time of crystallization to derive the Pb isotope composition of their source:

$$\left(\frac{^{206}Pb}{^{204}Pb}\right)_t = \left(\frac{^{206}Pb}{^{204}Pb}\right)_{today} - \mu \times \left(e^{(\lambda^{238}U \times t)} - 1\right) \quad (14)$$

$$\left(\frac{^{207}Pb}{^{204}Pb}\right)_t = \left(\frac{^{207}Pb}{^{204}Pb}\right)_{today} - \frac{\mu}{137.818} \times \left(e^{(\lambda^{235}U \times t)} - 1\right) \quad (15)$$

$$\left(\frac{^{208}Pb}{^{204}Pb}\right)_t = \left(\frac{^{208}Pb}{^{204}Pb}\right)_{today} - (\mu \times \kappa) \times \left(e^{(\lambda^{232}U \times t)} - 1\right) \quad (16)$$

For Pb isotope age correction, we use the decay constants of ^{238}U, ^{235}U, and ^{232}Th of Jaffey et al. (1971); Le Roux and Glendenin (1963), with $^{238}U/^{235}U = 137.818$ (Hiess et al., 2012).

To track the Pb isotope composition of the mantle throughout Earth's

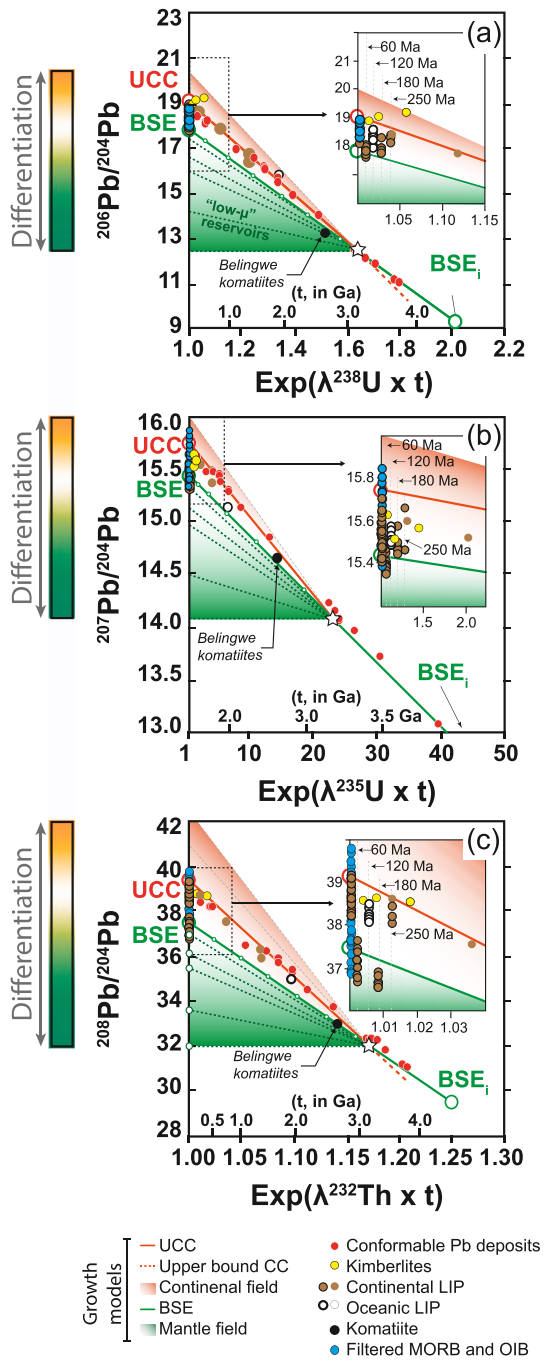

Fig. 13. Secular evolution of Pb isotopes on an Albarède-Martine diagram for conformable Pb ores, komatiite, oceanic and continental LIPs, kimberlites, present-day MORBs, and OIBs and LIPs with primordial signature relative to the Bulk Silicate Earth (solid green line), continental crust (solid orange line) and complementary low-μ mantle reservoirs (dashed green lines) growth models: age (as a function of exp.(λt)) vs. Pb ^{206}Pb/^{204}Pb (a), ^{207}Pb/^{204}Pb (b) and ^{208}Pb/^{204}Pb (c) (Albarede and Martine, 1984). The orange-to-green gradient field shows the range for possible Pb growth evolution after 3.2 Ga. The values for λ are the radioactive decay constants for ^{235}U, ^{238}U, ^{232}Th, and **t** is age in Ga. (For interpretation of the references to colour in this figure legend, the reader is referred to the web version of this article.)

history, we investigate data from mantle-derived rocks of the entire geological record in the literature. Such work requires (1) robust melting age estimates for the melt extraction, (2) U, Th, and Pb contents of the rocks, (3) good knowledge of possible contamination of the Pb isotopes by external reservoirs (e.g., by older oceanic or continental crust) and (4) evidence that the U/Pb and Th/U were not modified by contamination or by post-formation processes such as weathering or metamorphism. For the Cenozoic, abundant suitable MORB and OIB samples can be used. Further back in Earth history, such rocks have only been sporadically preserved. Continental large igneous provinces (LIPs) and kimberlites can potentially be used to track the Pb isotope composition of their respective mantle sources at the time of their formation (Bryan and Ernst, 2008; Ringwood et al., 1992), although post-melting processes (both during and after their emplacement) may obliterate their primary Pb isotopic compositions.

Here, all the Pb isotopic data from ancient rocks is filtered the same way as for oceanic basalts (see section 4.1) (Tables 4 and 5, and Supplementary Data Table 4). Importantly, we note that the Pb isotope compositions of all these rocks generally plot between the UCC and BSE Pb isotope growth lines (Fig. 13). Nonetheless, some OIB and continental LIP samples show primordial signatures (Jackson and Carlson, 2011; Wang et al., 2013) (Fig. 9), and along with the 2.7 Ga Belingwe (Zimbabwe; Table 4) komatiite and some MORB samples, they plot below the BSE Pb isotope growth curve (Fig. 13a), implying that they represent mantle reservoirs that were depleted by the extraction of the continental crust. Therefore, the Pb composition and evolution of mantle-derived rocks appear to have inherited an intrinsic heterogeneity caused by both differentiation processes and remixing in their source(s). Consequently, each mantle-derived rock could potentially represent a reservoir with a distinct mixture of differentiation and remixing processes, making it impossible to uniquely describe the evolutionary path of mantle-derived rocks using a single Pb growth line (Fig. 13). Our model bears some similarities with the hidden mantle reservoir model of Malaviarachchi et al. (2008) and Burton et al. (2012) (see section 2.1.4), but we emphasize the likely presence of multiple, variably depleted, and mostly hidden mantle reservoirs.

5. Implication for a dynamic evolution of the silicate Earth

An evolutionary step change in the Pb isotopic composition trend of galena at 3.2 Ga implies that significant U/Pb and Th/U fractionation occurred in the sources of Pb deposits. This time coincides with the proposed transition of Earth's tectonic regime from a dominantly stagnant lid mode (Stern et al., 2018) to a mobile-lid mode akin to our present-day plate tectonics (Brenner et al., 2020; Dhuime et al., 2012; Gamaleldien et al., 2020; Hartnady and Kirkland, 2019; Kirkland et al., 2021; Shirey and Richardson, 2011; Van Kranendonk et al., 2007). Progressive cooling of Earth's mantle during the Archean resulted in thinning of oceanic lithosphere and a decrease in its buoyancy (Herzberg et al., 2010; Palin and White, 2016), which ultimately promoted the transition from a stagnant lid regime to one dominated by subduction at ca. 3.2–3.0 Ga (Palin et al., 2020; Shirey and Richardson, 2011). The initiation of global and whole-mantle subduction-related mantle remixing from ca. 3.2 Ga (Gamaleldien et al., 2020), possibly associated with global plate tectonics, was accompanied by the rapid growth of continental crustal during ~3.2–3.0 Ga (Kirkland et al., 2021) and thus the addition of high volumes of radiogenic elements to the continental crust (McDonough, 2007). Therefore, it appears as little coincidence that the global Pb isotope data started to follow a growth curve of the continental crust after 3.2 Ga (Fig. 12).

Our work provides a new framework for understanding the diverse evolutionary paths of Earth materials and their source domains, whether sampled or not. Traditionally, the evolution of the BSE is often confused with that of the continental crust. For example, the classical Pb growth model of Stacey and Kramers (1975), based on conformable terrestrial Pb deposits, has often been used as representing the BSE evolution (Hofmann, 2001) (see section 3.2). We demonstrate here that the Earth's continental crust has a distinct evolutionary curve from that of the BSE, and the model of Stacey and Kramers (1975) applies to the continental crust as an average value only (including most of the continental LIPs and kimberlites) (Figs. 12e and 13). For mantle rocks, the new BSE curve

Table 4
List of available mafic samples in the geological record with Pb isotopes with reported U, Pb and Th contents.

Location	Ages (Ma)	Number of samples	Sample with	References
	Ma		$\kappa \sim \kappa Pb$ (±0.2)	
Siberian traps	250	8	0	Kogarko and Zartman (2007)
Emeishan LIP	260	105	23	Fan et al. (2008); Lai et al. (2012); Li et al. (2017); Thi et al. (2014); Xiao et al. (2003); Xu et al. (2007); Zhang et al. (2006); Zhang et al., 2009; Zhang et al., 2008
Kalkarindji LIP	511	10	0	Ware et al. (2018)
Franklin LIP	720	10	1	Dupuy et al. (1995)
Midsommersø LIP	1380	26	5	Kalsbeek and Frei (2006)
Hart River Sills	1380	7	1	Verbaas et al. (2018)
Flin Flon LIP	1900	43	5	Babechuk and Kamber (2011)
Zimbabwe (LIP?)	2700	8	5	Shimizu et al. (2005)
Kimberlites	1090–80	87	10	Bogatikov et al. (2004); Bogatikov et al. (2001); Conceição et al. (2019); Eccles et al. (2004); Fraser and Hawkesworth (1992); Golubeva et al. (2004); Kononova et al. (2005); Kramers (1977); Schmidberger and Francis (1999); Tappe et al. (2017)

Table 5
Secular Pb isotopic composition of mantle-derived continental large igneous provinces and kimberlites: the average of isotopic composition for each period.

Age (Ma)	$^{206}Pb/^{204}Pb_{(t)}$	$^{207}Pb/^{204}Pb_{(t)}$	$^{208}Pb/^{204}Pb_{(t)}$
90	18.85	15.62	38.6
160	19.01	15.51	38.6
200	19.16	15.56	38.55
260	18.41	15.59	38.58
360	19.16	15.56	38.55
720	17.75	15.51	37.53
1090	12.25	15.03	31.90
1380	16.24	15.35	35.99
1380	16.42	15.46	36.12
1900	15.70	15.11	34.90
2700	13.15	14.62	32.88

(t) Pb isotope composition corrected from age of eruption. Reference from Table 4.

is a better approximation for non-differentiated BSE values with time (Figs. 10, 12, and 13). In reality, mantle rocks are expected to fall on an infinite number of different Pb evolution curves, driven by varying degrees of differentiation, as illustrated by the colour lines/zoning in Figs. 13–16. Further complexity is caused by both mixing of various components and fractionation processes after 3.2 Ga (Figs. 13, 16). The importance of the latter processes is illustrated in Fig. 14, where Cenozoic data points are scattered to both the left and the right sides of the theoretical "present-day" differentiation line.

This new global Pb isotope framework provides a solution to the first Pb paradox in that even though the Pb isotopic values of present-day Earth materials mostly plot to the right of the geochron (Figs. 14 and 16), to a first-order, they lie on the Pb differentiation line defined by present-day BSE and continental crust (Figs. 14 and 16). The fact that the data plot mostly to the right of the geochron reflects second-order

Table 6
Parameters defining the Bulk Silicate Earth and continental crust Pb isotope growth curves of this study.

	Time	$^{238}U/^{204}Pb$ or μ	$^{232}Th/^{238}U$ or ϰ	$^{206}Pb/^{204}Pb$	$^{207}Pb/^{204}Pb$	$^{208}Pb/^{204}Pb$
BSE	4.504 Ga	8.41	3.9	9.338	10.355	29.50
	today			17.84	15.44	37.72
UCC	3.2 Ga	10.104	4.2	12.435	14.08	31.995
	today			18.93*	15.71*	39.03*

Calculations can be reproduced using Matlab code in Research Data 1.
* Data from Millot et al. (2004).

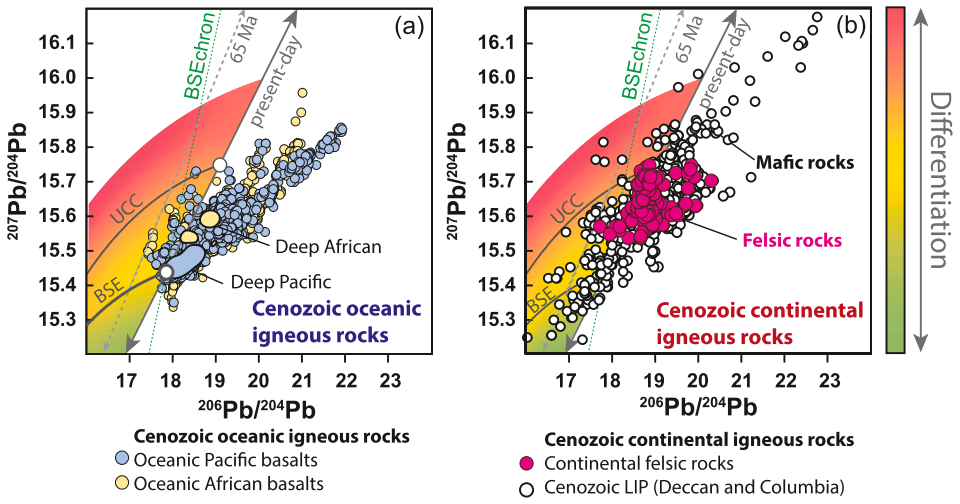

Fig. 14. Pb isotope composition of Cenozoic oceanic and continental igneous rocks. (a) $^{206}Pb/^{204}Pb$ vs $^{207}Pb/^{204}Pb$ for Cenozoic oceanic basalts from the African and Pacific domains (Doucet et al., 2020b), and (b) Cenozoic continental mafic and felsic rocks. All data are from the Earthchem Portal (http://portal.earthchem.org/). Also shown are the BSEchron and the growth model presented in this study (Table 6). The fields for mantle-plume derived basalts with deep origin (90 percentile) is from Doucet et al. (2020b).

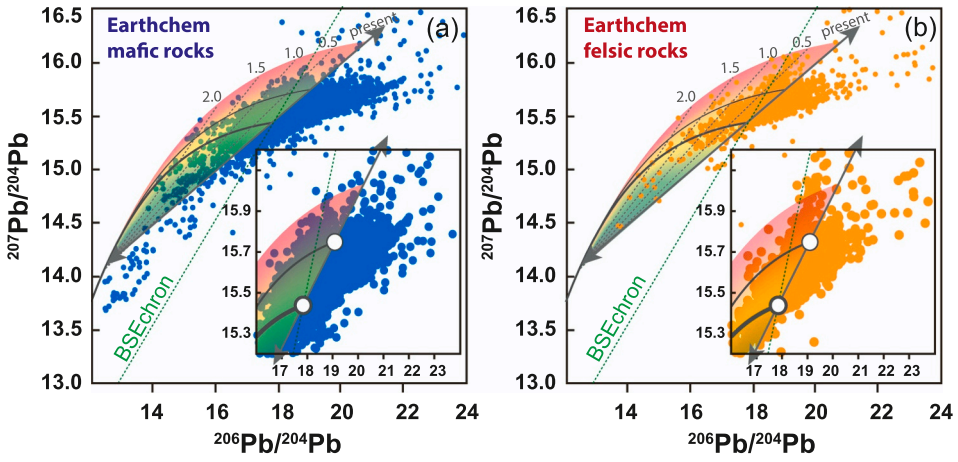

Fig. 15. Pb isotope compositions for mafic igneous rocks (a) and felsic igneous rocks (b). The $^{206}Pb/^{204}Pb$ and $^{207}Pb/^{204}Pb$ data are from the Earthchem Portal (https://www.earthchem.org/).

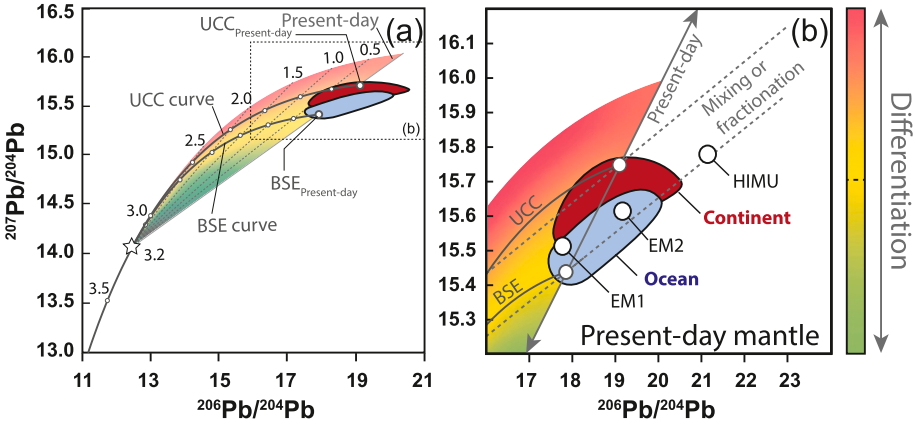

Fig. 16. Figure illustrating the new Lead isotope evolution framework of this study, emphasizing the importance of Earth's differentiation (shown in grading colour shades), and remixing and fractionation. The $^{206}Pb/^{204}Pb$ vs $^{207}Pb/^{204}Pb$ reference frame for the present-day oceanic and continental igneous rocks (Table 6) is compared to the estimates for HIMU, EM1, and EM2 endmembers.

complications caused by both source mixing and fractionation of Earth materials (Fig. 16). These observations imply that rocks found on Earth's surface mostly originated from more radiogenic (with HIMU being an end member) reservoirs, probably at shallower levels (the upper mantle and the crust) where long-term gravitational differentiation and subduction-led mantle remixing preferentially concentrated more radiogenic materials. Furthermore, the second Pb paradox (the "kappa conundrum"; Elliott et al. (1999)) is significantly mitigated by demonstrating that the κ vs. κ_{Pb} plot, using an updated global database, shows a near-symmetric normal distribution of κ around a consistent κ_{Pb} value, with the scattering of the κ values interpreted to reflect open system behavior of some of the samples/mantle sources (section 2.2).

6. Implication for common Pb correction and absolute U-Th-Pb dating

6.1. The effect of common Pb on U-Th-Pb dating

The U-Th-Pb system has been used for more than a hundred years (Holmes, 1911) and revolutionized our understanding of geological processes (Schoene, 2014). Uranium-bearing minerals are ubiquitous in most rocks (sedimentary, igneous, and metamorphic rocks) and many are resistant to chemical and physical weathering (Hoskin and Schaltegger, 2003), which explains the popularity and number of publications reporting U-Pb dating (>8800 articles recorded in www.webofknowledge.com) (Spencer et al., 2016). Zircon is by far the most common mineral used for U-Pb dating, because Pb is rarely incorporated into the mineral during formation, with almost all measured Pb being the daughter products of radioactive decay of U and Th. The minute volumes of so-called 'common Pb' in most zircon grains mean that direct measurement of U-Pb reflects the age of the geological event of interest (e.g., crystallization, metamorphism). The only exception is where zircon becomes metamict due to α-radiation damage during radioactive decay of the U and Th to Pb (Murakami et al., 1991), but these grains rarely give any meaningful U-Pb results and so are generally of little concern. Other minerals such as monazite, xenotime, and baddeleyite behave similarly to zircon in that they mostly incorporate negligible common Pb during crystallization.

However, zircon can still incorporate a small amount of common Pb (<1.5%, unless metamict, Fig. 17a), and other minerals such as apatite and titanite certainly contain higher common Pb cargos which can affect the accuracy of dating if not accounted for. Depending on the analytical technique used for dating, the proportion of common Pb (measured as $^{206}Pb/^{204}Pb$, $^{207}Pb/^{204}Pb$, and $^{208}Pb/^{204}Pb$) can be subtracted from the total Pb but this requires a model, or a good estimation, of the primary Pb composition. So far, the most popular way to correct for common Pb in zircon and other phases with small proportions of common Pb is to (1) estimate the concentration of common Pb using the stable isotope of Pb (^{204}Pb), and (2) estimate common Pb isotopic composition at the approximate time of crystallization using the Pb isotopic growth model

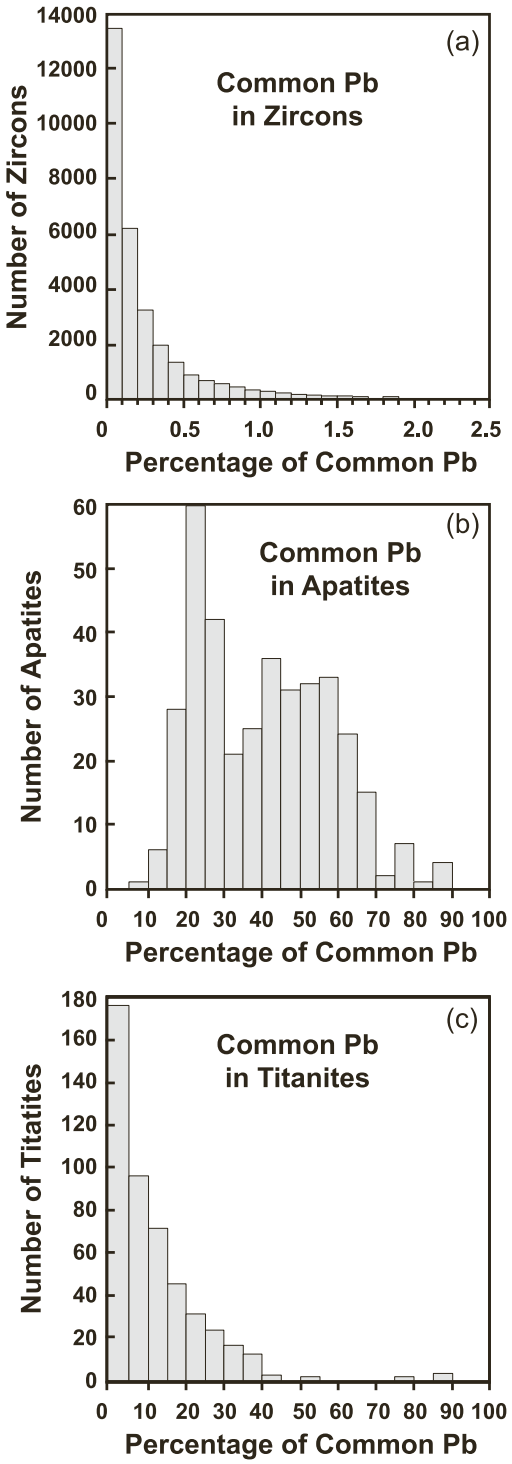

Fig. 17. Common Pb cargo, shown by histograms of the percentage of common Pb, in zircons (a), apatite (b), and titanites (c). The percentage of common Pb in zircons is measured by analyzing ^{204}Pb during Curtin University SHRIMP analyses. Percentage of common Pb in apatites and titanite is estimated using arithmetic solution in the Tera-Wasserburg Concordia diagram (Tera and Wasserburg, 1972a; Tera and Wasserburg, 1972b). The data are from the John De Leater Research Center of Curtin University and are available upon request.

of Stacey and Kramers (1975) (e.g., Andersen, 2002; Williams, 1997). As we discussed in section 4, our new models for BSE and UCC allow us to refine common Pb correction and evaluation for the two generalized earth reservoirs (and theoretically, a unique model can be defined for a range of more finely defined reservoirs). Overall, the common Pb isotopic evolution for UCC as we defined here is similar to the second stage model of Stacey and Kramers (1975) (Fig. 18a), still, significant errors might occur if the Stacey and Kramers (1975) model is applied for common Pb correction of zircon derived from continental material with ages younger than 1.0 Ga (Fig. 18c). For example, a 500 Ma continental crust-derived zircon grain with 1% common Pb (the typical maximum for common Pb corrections) will be ~15 m.y. too young if the model of Stacey and Kramers (1975) was used (Fig. 18c). On the other hand, in the case of mantle-derived zircons (or baddeleyite), that can form in the lower-crustal section of oceanic crust, oceanic plateaus, seamounts, and ocean islands, and in evolved magmas such as kimberlite and lamproite, using the model of Stacey and Kramers (1975) instead of our mantle model could have a significant impact on the accuracy of the measured ages, dependent on the amount of common Pb (Fig. 18d). For example, a 500 Ma mantle-derived zircon grain with 1% common Pb would be dated ~150 m.y. too young if the model of Stacey and Kramers (1975) were used (Fig. 18d). The age difference becomes increasingly greater for younger mantle-derived zircon grains, due to both the discrepancy between models and the reduced time for radiogenic ingrowth of Pb.

Other minerals used for U-Th-Pb dating also incorporate appreciable amounts of common Pb (e.g., titanite, rutile, apatite, allanite, perovskite; Fig. 17b, c). For such high common Pb minerals, the most common approach is to fit regressions through the 'uncorrected' data on a Tera-Wasserburg inverse Concordia curve (Tera and Wasserburg, 1972a), effectively defining a mixing line between common and radiogenic Pb components. The lower intercept with the Concordia curve then defines the age of closure to radiogenic-Pb diffusion, whereas the intercept with the ordinate axis (^{207}Pb/^{206}Pb) defines the composition of the common Pb reservoir(Tera and Wasserburg, 1972a; Tera and Wasserburg, 1972b). As this method does not require any assumptions of the composition of the common Pb reservoir, it is largely immune to the model-based common Pb correction problems explained above, but rather has the assumption that all analyses sourced the same common Pb reservoir which may not be accurate.

6.2. *The Pb-Pb model ages*

The new UCC Pb isotope model gives similar secular isotopic evolution as the second stage of Stacey and Kramer's (1975) model after 3.2 Ga (Fig. 18a) and therefore yields simil Pb-Pb model ages (i.e., ±50 Ma; Fig. 18b). Before 3.2 Ga, the new BSE model gives Pb-Pb ages that reproduce stratigraphic ages of conformable Pb deposits (Table 3). The new UCC growth model provides similar results as the model ages calculated using Stacey and Kramers (1975) for continental-derived Pb deposits. The new BSE growth model, however, offers a refined and more accurate model for mantle-derived deposits.

7. Conclusions

Lead isotopes allow for the characterization of the origin and tracking the diverse evolutionary paths of most materials in the silicate Earth, from its upper crust to the basal mantle. Such a diversity of reservoirs reflects the combination of Earth's long-term differentiation processes, its dynamic whole-mantle remixing since the large-scale extraction of continental crust and the start of global plate tectonics at ca. 3.2 Ga, and its fractionation processes (Fig. 16). Earth's mantle is characterized by heterogeneity across multiple scales, and mantle-derived rocks therefore cannot be entirely described by a previously proposed single Pb isotopic growth curve (Cumming and Richards, 1975; Maltese and Mezger, 2020; Stacey and Kramers, 1975). This new framework provides a powerful tool for documenting and understanding Earth's dynamic history through characterizing and analyzing all available Earth materials, from mantle xenoliths, igneous rocks of both the oceanic and continental realms, to other continental rocks; for example, using the mantle record to track down the existence and evolution history of long-wavelength mantle domains and establish the

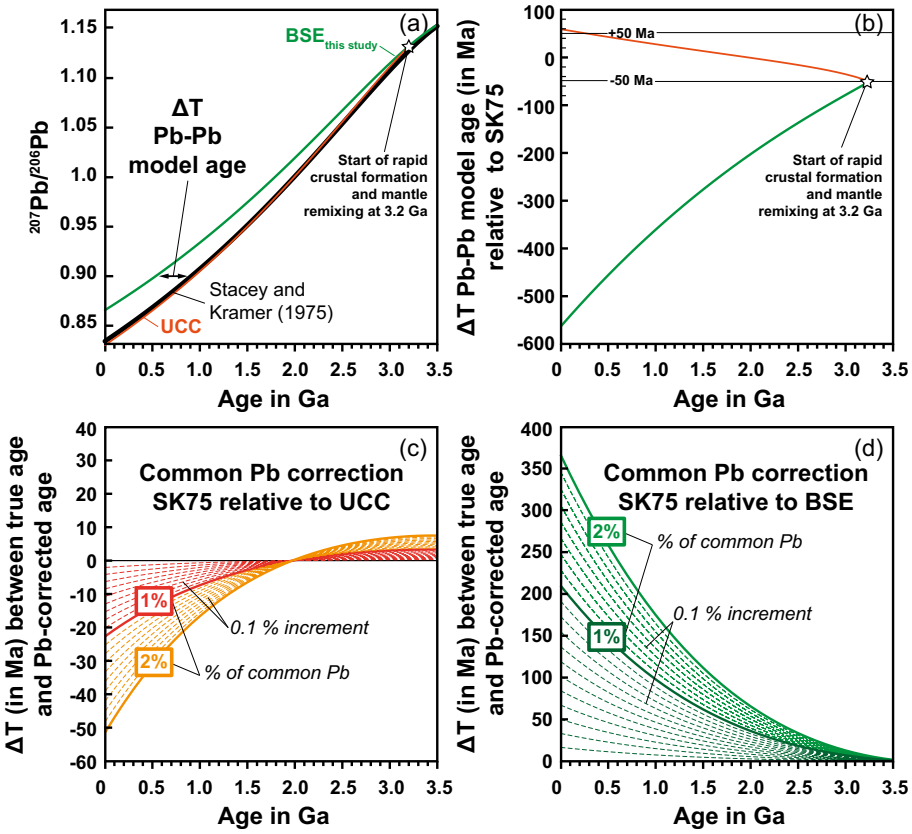

Fig. 18. Effect of the new BSE and UCC growth model on common Pb correction and Pb-Pb model ages: (a) secular evolution of $^{207}Pb/^{206}Pb$ for BSE and UCC compared to the second-stage growth model of Stacey and Kramer (1975), (b) difference in Pb-Pb model ages between those using the new BSE and UCC growth model and those using the second-stage growth model of Stacey and Kramer (1975), (c) difference in resulting U-Pb ages for continental crust zircons between those performing common Pb correction using the Stacey and Kramers (1975) model and those using the new Pb growth curve for the UCC reservoir, and (d) difference in resulting U-Pb ages for mantle-derived zircons between those performing common Pb correction using the Stacey and Kramers (1975) nodel and those using the new Pb growth curve for the BSE reservoir.

tectonic and geodynamic history of supercontinent cycles (Doucet et al., 2020a; Doucet et al., 2020b; Li et al., 2019; Gamaleldien et al., 2019). The new understanding of unique Pb isotopic growth curves for each individual mantle domain has potentially profound implications for the choice of Pb model when applying a correction for non-radiogenic Pb in U-Pb dating of mantle-derived rocks.

Code availability

The figures were produced using a MATLAB script which is available in Researchg Data 1 or upon request to the corresponding authors.

Declaration of Competing Interest

The authors declare the following financial interests/personal relationships which may be considered as potential competing interests:

Doucet reports a relationship with Curtin University that includes: employment.

Data availability

All of the data used in this study can be found directly in the related papers for the Pb isotopes of stratiform Pb ore deposits, the Earthchem Portal for the Pb isotopes of igneous rocks, and on the Geoscience Australia website for the compilation of the Australian Galena.

Acknowledgements

We thank Josh Beardmore for proofreading. We thank Z.-J. Zhang and three anonymous reviewers, and Tim Kusky for editorial handling. This work was supported by the Australian Research Council Laureate Fellowship grant to Z.X.L. (FL150100133). We thank the two anonymous reviewers for their comments that helped to improve this contribution. This article is a contribution to IGCP 648 "*Supercontinent cycles and global geodynamics*".

Appendix A. Supplementary data

Supplementary data to this article can be found online at https://doi.org/10.1016/j.earscirev.2023.104483.

References

Alard, O., Luguet, A., Pearson, N.J., Griffin, W.L., Lorand, J.-P., Gannoun, A., Burton, K. W., O'Reilly, S.Y., 2005. In situ Os isotopes in abyssal peridotites bridge the isotopic gap between MORBs and their source mantle. Nature 436 (7053), 1005–1008.
Albarede, F., 2009. Volatile accretion history of the terrestrial planets and dynamic implications. Nature 461 (7268), 1227–1233.
Albarede, F., Martine, J., 1984. Unscrambling the lead model ages. Geochim. Cosmochim. Acta 48 (1), 207–212.
Allègre, C.J., 1968. Comportement des systèmes U-Th-Pb dans le manteau supérieur et modèle d'évolution de ce dernier au cours des temps géologiques. E&PSL 5, 261–269.
Allègre, C.J., Dupré, B., Brévart, O., 1982. Chemical aspects of the formation of the core. Phil. Trans. R. Soc. Lond. Ser. A Math. Phys. Sci. 306 (1492), 49–59.
Allègre, C.J., Dupré, B., Lewin, E., 1986. Thorium/uranium ratio of the Earth. Chem. Geol. 56 (3–4), 219–227.
Allègre, C.J., Hofmann, A., O'Nions, K., 1996. The argon constraints on mantle structure. Geophys. Res. Lett. 23 (24), 3555–3557.
Allègre, C.J., Lewin, E., 1989. Chemical structure and history of the Earth: evidence from global non-linear inversion of isotopic data in a three-box model. Earth Planet. Sci. Lett. 96 (1–2), 61–88.
Allègre, C.J., Lewin, E., Dupré, B., 1988. A coherent crust-mantle model for the uranium-thorium-lead isotopic system. Chem. Geol. 70 (3), 211–234.
Allegre, C.J., Manhes, G., Göpel, C., 1995. The age of the Earth. Geochim. Cosmochim. Acta 59 (8), 1445–1456.
Allègre, C.J., Staudacher, T., Sarda, P., Kurz, M., 1983. Constraints on evolution of Earth's mantle from rare gas systematics. Nature 303 (5920), 762.
Andersen, M.B., Elliott, T., Freymuth, H., Sims, K.W., Niu, Y., Kelley, K.A., 2015. The terrestrial uranium isotope cycle. Nature 517 (7534), 356–359.
Andersen, T., 2002. Correction of common lead in U-Pb analyses that do not report 204Pb. Chem. Geol. 192 (1–2), 59–79.

Andrieu, A., Honnorez, J., Lancelot, J., 1998. Lead isotope compositions of the TAG mineralization, Mid-Atlantic Ridge, 26 08′ N. In: Proceedings of the Ocean Drilling Program, Scientific Results, pp. 101–109.
Asmerom, Y., Jacobsen, S.B., 1993. The Pb isotopic evolution of the Earth: inferences from river water suspended loads. Earth Planet. Sci. Lett. 115 (1–4), 245–256.
Bea, F., Montero, P., 1999. Behavior of accessory phases and redistribution of Zr, REE, Y, Th, and U during metamorphism and partial melting of metapelites in the lower crust: an example from the Kinzigite Formation of Ivrea-Verbano, NW Italy. Geochim. Cosmochim. Acta 63 (7–8), 1133–1153.
Benz, W., Cameron, A., Melosh, H., 1989. The origin of the Moon and the single-impact hypothesis III. Icarus 81 (1), 113–131.
Benz, W., Slattery, W., Cameron, A., 1986. The origin of the Moon and the single-impact hypothesis I. Icarus 66 (3), 515–535.
Benz, W., Slattery, W., Cameron, A., 1987. The origin of the Moon and the single-impact hypothesis, II. Icarus 71 (1), 30–45.
Blichert-Toft, J., Zanda, B., Ebel, D.S., Albarède, F., 2010. The solar system primordial lead. Earth Planet. Sci. Lett. 300 (1–2), 152–163.
Bouvier, A., Wadhwa, M., 2010. The age of the Solar System redefined by the oldest Pb–Pb age of a meteoritic inclusion. Nat. Geosci. 3 (9), 637–641.
Boyd, F.R., 1970. Garnet peridotites and the system CaSiO3-MgSiO3-Al2O3. Mineral Soc. Amer. Spec. Pap. 3, 63–75.
Boyd, F.R., 1989. Compositional distinction between oceanic and cratonic lithosphere. Earth Planet. Sci. Lett. 96, 15–26.
Boyet, M., Carlson, R.W., 2005. 142Nd evidence for early (> 4.53 Ga) global differentiation of the silicate Earth. Science 309 (5734), 576–581.
Brenner, A.R., Fu, R.R., Evans, D.A., Smirnov, A.V., Trubko, R., Rose, I.R., 2020. Paleomagnetic evidence for modern-like plate motion velocities at 3.2 Ga. Sci. Adv. 6 (17), eaaz8670.
Bryan, S.E., Ernst, R.E., 2008. Revised definition of large Igneous Provinces (LIPs). Earth Sci. Rev. 86 (1–4), 175–202.
Burkhardt, C., Borg, L., Brennecka, G., Shollenberger, Q., Dauphas, N., Kleine, T., 2016. A nucleosynthetic origin for the Earth's anomalous 142Nd composition. Nature 537 (7620), 394–398.
Burton, K.W., Cenki-Tok, B., Mokadem, F., Harvey, J., Gannoun, A., Alard, O., Parkinson, I.J., 2012. Unradiogenic lead in Earth's upper mantle. Nat. Geosci. 5 (8), 570–573.
Cameron, A., 1997. The origin of the Moon and the single impact hypothesis V. Icarus 126 (1), 126–137.
Cameron, A., Benz, W., 1991. The origin of the Moon and the single impact hypothesis IV. Icarus 92 (2), 204–216.
Campbell, I.H., O'Neill, St C., 2012. Evidence against a chondritic Earth. Nature 483 (7391), 553–558.
Canup, R.M., Asphaug, E., 2001. Origin of the Moon in a giant impact near the end of the Earth's formation. Nature 412 (6848), 708–712.
Caro, G., Bourdon, B., Halliday, A.N., Quitté, G., 2008. Super-chondritic Sm/Nd ratios in Mars, the Earth and the Moon. Nature 452 (7185), 336–339.
Castillo, P., MacIsaac, C., Perry, S., Veizer, J., 2018. Marine carbonates in the mantle source of oceanic basalts: Pb isotopic constraints. Sci. Rep. 8 (1), 1–7.
Castillo, P.R., 2015. The recycling of marine carbonates and sources of HIMU and FOZO Ocean island basalts. Lithos 216, 254–263.
Chauvel, C., Goldstein, S.L., AW, H., 1995. Hydration and dehydration of oceanic crust controls Pb evolution in the mantle. Chem. Geol. 126, 65–75.
Collerson, K.D., Kamber, B.S., 1999. Evolution of the continents and the atmosphere inferred from Th-U-Nb systematics of the depleted mantle. Science 283 (5407), 1519–1522.
Connelly, J., Bizzarro, M., 2016. Lead isotope evidence for a young formation age of the Earth-Moon system. Earth Planet. Sci. Lett. 452, 36–43.
Cooper, J., Reynolds, P., Richards, J., 1969. Double-spike calibration of the Broken Hill standard lead. Earth Planet. Sci. Lett. 6 (6), 467–478.
Cumming, G., Richards, J., 1975. Ore lead isotope ratios in a continuously changing Earth. Earth Planet. Sci. Lett. 28 (2), 155–171.
Dauphas, N., 2017. The isotopic nature of the Earth's accreting material through time. Nature 541 (7638), 521–524.
Davies, G.F., 1984. Geophysical and isotopic constraints on mantle convection: an interim synthesis. J. Geophys. Res. Solid Earth 89 (B7), 6017–6040.
Dhuime, B., Hawkesworth, C.J., Cawood, P.A., Storey, C.D., 2012. A Change in the Geodynamics of Continental Growth 3 billion years Ago. Science 335 (6074), 1334–1336.
Doe, B., Zartman, R., 1979. Geochemistry of hydrothermal ore deposits. John Wiley and Sons.
Doucet, L., Ionov, D., Golovin, A., 2013. The origin of coarse garnet peridotites in cratonic lithosphere: new data on xenoliths from the Udachnaya kimberlite, Central Siberia. Contrib. Mineral. Petrol. 165 (6), 1225–1242.
Doucet, L.S., Ionov, D.A., Golovin, A.V., Pokhilenko, N.P., 2012. Depth, degrees and tectonic settings of mantle melting during craton formation: inferences from major and trace element compositions of spinel harzburgite xenoliths from the Udachnaya kimberlite, Central Siberia. Earth Planet. Sci. Lett. 359–360, 206–218.
Doucet, L.S., Li, Z.-X., Ernst, R.E., Kirscher, U., Gamaleldien, H., Mitchell, R.N., 2020a. Coupled supercontinent–mantle plume events evidenced by oceanic plume record. Geology 48 (2), 159–163.
Doucet, L.S., Li, Z.-X., Gamaleldien, H., Pourteau, A., Murphy, J.B., Collins, W.J., Mattielli, N., Olierook, H.K.H., Spencer, C.J., Mitchell, R.N., 2020b. Distinct formation history for deep-mantle domains reflected in geochemical differences. Nat. Geosci. 13 (7), 511–515.
Dupré, B., Allègre, C.J., 1983. Pb-Sr isotope variations in Indian Ocean basalts and mixing phenomena. Nature 303, 142–146.
Elliott, T., Zindler, A., Bourdon, B., 1999. Exploring the kappa conundrum: the role of recycling in the lead isotope evolution of the mantle. Earth Planet. Sci. Lett. 169 (1–2), 129–145.
Fisher, C.M., Vervoort, J.D., 2018. Using the magmatic record to constrain the growth of continental crust—The Eoarchean zircon Hf record of Greenland. Earth Planet. Sci. Lett. 488, 79–91.
Flament, N., Bodur, Ö.F., Williams, S.E., Merdith, A.S., 2022. Assembly of the basal mantle structure beneath Africa. Nature 603 (7903), 846–851.
Fouquet, Y., Marcoux, E., 1995. Lead isotope systematics in Pacific hydrothermal sulfide deposits. J. Geophys. Res. Solid Earth 100 (B4), 6025–6040.
Frossard, P., Israel, C., Bouvier, A., Boyet, M., 2022. Earth's composition was modified by collisional erosion. Science 377 (6614), 1529–1532.
Fukao, Y., Obayashi, M., 2013. Subducted slabs stagnant above, penetrating through, and trapped below the 660 km discontinuity. J. Geophys. Res. Solid Earth 118 (11), 5920–5938.
Galer, S., Goldstein, S., 1991. Early mantle differentiation and its thermal consequences. Geochim. Cosmochim. Acta 55 (1), 227–239.
Galer, S., O'Nions, R., 1985. Residence time of thorium, uranium and lead in the mantle with implications for mantle convection. Nature 316 (6031), 778–782.
Galer, S.J., Goldstein, S.L., 1996. Influence of accretion on lead in the Earth. Geophys. Monogr.Am. Geophys. Union 95, 75–98.
Gamaleldien, H., Doucet, L.S., Li, Z.-X., Cox, G., Mitchell, R., 2019. Global geochemical fingerprinting of plume intensity suggests coupling with the supercontinent cycle. Nat. Commun. 10, 5270. https://doi.org/10.1038/s41467-019-13300-4.
Gamaleldien, H., Doucet, L.S., Murphy, J.B., Li, Z.-X., 2020. Geochemical evidence for a widespread mantle re-enrichment 3.2 billion years ago: implications for global-scale plate tectonics. Sci. Rep. 10 (1), 1–7.
Goes, S., Agrusta, R., van Hunen, J., Garel, F., 2017. Subduction-transition zone interaction: A review. Geosphere 13 (3), 644–664.
Halliday, A.N., 2004. Mixing, volatile loss and compositional change during impact-driven accretion of the Earth. Nature 427 (6974), 505–509.
Halliday, A.N., Canup, R.M., 2023. The accretion of planet Earth. Nat. Rev. Earth Environ. 4 (1), 19–35.
Harrison, T.M., 2020. In: The Lunar Surface and Late Heavy Bombardment Concept, Hadean Earth. Springer, pp. 59–100.
Hart, S.R., 1984. A large-scale anomaly in the Southern Hemisphere mantle. Nature 309, 753–757.
Hartnady, M.I., Kirkland, C.L., 2019. A gradual transition to plate tectonics on Earth between 3.2 to 2.7 billion years ago. Terra Nova 31 (2), 129–134.
Hartnady, M.I., Kirkland, C.L., Smithies, R.H., Johnson, S.P., Johnson, T.E., 2022. Pb isotope insight into the formation of the Earth's first stable continents. Earth Planet. Sci. Lett. 578, 117319.
Hasenstab-Dübeler, E., Münker, C., Tusch, J., Thiemens, M., Garbe-Schönberg, D., Strub, E., Sprung, P., 2023. Cerium-Nd isotope evidence for an incompatible element depleted Moon. Earth Planet. Sci. Lett. 606, 118018.
Heinrich, C.A., Candela, P.A., 2014. Fluids and ore formation in the Earth's crust, Treatise on Geochemistry. In: Second edition. Elsevier, pp. 1–28.
Herzberg, C., Condie, K., Korenaga, J., 2010. Thermal history of the Earth and its petrological expression. Earth Planet. Sci. Lett. 292 (1–2), 79–88.
Hiess, J., Condon, D.J., McLean, N., Noble, S.R., 2012. 238U/235U systematics in terrestrial uranium-bearing minerals. Science 335 (6076), 1610–1614.
Hofmann, A.W., 2001. Lead isotopes and the age of the Earth—a geochemical accident. Geol. Soc. Lond. Spec. Publ. 190 (1), 223–236.
Hofmann, A.W., White, W.M., 1982. Mantle plumes from ancient oceanic crust. Earth Planet. Sci. Lett. 57, 421–436.
Holmes, A., 1911. The association of lead with uranium in rock-minerals, and its application to the measurement of geological time. Proc. R. Soc. Lond. 85 (578), 248–256.
Holmes, A., 1913. The age of the Earth.
Holmes, A., 1946. An estimate of the age of the Earth. Nature 157 (3995), 680–684.
Holmes, A., 1947a. An estimate of the age of the Earth. Geol. Mag. 84 (2), 123–126.
Holmes, A., 1947b. A revised estimate of the age of the earth. Nature 159 (4030), 127–128.
Hoskin, P.W., Schaltegger, U., 2003. The composition of zircon and igneous and metamorphic petrogenesis. Rev. Mineral. Geochem. 53 (1), 27–62.
Houtermans, F.G., 1953. Determination of the age of the earth from the isotopic composition of meteoritic lead. Il Nuovo Cimento (1943-1954) 10 (12), 1623–1633.
Hurley, P.M., Fairbairn, H.W., 1957. Abundance and distribution of uranium and thorium in zircon, sphene, apatite, epidote, and monazite in granitic rocks. Eos Trans. Am. Geophys. Union 38 (6), 939–944.
Huston, D.L., Champion, D.C., Ware, B., Carr, G., Maas, R., Tessalina, S.G., 2019. Preliminary national-scale lead isotope maps of Australia. Geosci. Aust.
Jackson, M.G., Blichert-Toft, J., Halldórsson, S.A., Mundl-Petermeier, A., Bizimis, M., Kurz, M.D., Price, A.A., Harðardóttir, S., Willhite, L.N., Breddam, K., 2020. Ancient helium and tungsten isotopic signatures preserved in mantle domains least modified by crustal recycling. Proc. Natl. Acad. Sci. 117 (49), 30993–31001.
Jackson, M.G., Carlson, R.W., 2011. An ancient recipe for flood-basalt genesis. Nature 476 (7360), 316–319.
Jackson, M.G., Carlson, R.W., Kurz, M.D., Kempton, P.D., Francis, D., Blusztajn, J., 2010. Evidence for the survival of the oldest terrestrial mantle reservoir. Nature 466 (7308), 853–856.
Jackson, M.G., Konter, J.G., Becker, T.W., 2017. Primordial helium entrained by the hottest mantle plumes. Nature 542, 340.
Jaffey, A., Flynn, K., Glendenin, L., Bentley, W.T., Essling, A., 1971. Precision measurement of half-lives and specific activities of U 235 and U 238. Phys. Rev. C 4 (5), 1889.

Kamber, B.S., Kramers, J.D., 2006. How well can Pb isotopes date core formation? Nature 444 (7115), E1–E2.
Kelley, K.A., Plank, T., Farr, L., Ludden, J., Staudigel, H., 2005. Subduction cycling of U, Th, and Pb. Earth Planet. Sci. Lett. 234 (3–4), 369–383.
Kirkland, C., Hartnady, M., Barham, M., Olierook, H., Steenfelt, A., Hollis, J., 2021. Widespread reworking of Hadean-to-Eoarchean continents during Earth's thermal peak. Nat. Commun. 12 (1), 1–9.
Kleine, T., Münker, C., Mezger, K., Palme, H., 2002. Rapid accretion and early core formation on asteroids and the terrestrial planets from Hf–W chronometry. Nature 418 (6901), 952–955.
Kramers, J.D., Tolstikhin, I.N., 1997. Two terrestrial lead isotope paradoxes, forward transport modelling, core formation and the history of the continental crust. Chem. Geol. 139 (1), 75–110.
Kruijer, T.S., Archer, G.J., Kleine, T., 2021. No 182W evidence for early Moon formation. Nat. Geosci. 14 (10), 714–715.
Kurz, M., Jenkins, W., Hart, S., 1982. Helium isotopic systematics of oceanic islands and mantle heterogeneity. Nature 297 (5861), 43.
Kwon, S., Tilton, G., Grunenfelder, M., Bell, K., 1989. Lead isotope relationships in carbonatites and alkalic complexes: an overview. In: Carbonatites: Genesis and Evolution, pp. 360–387.
Lassiter, J., Hauri, E., 1998. Osmium-isotope variations in hawaiian lavas: evidence for recycled oceanic lithosphere in the hawaiian plume. Earth Planet. Sci. Lett. 164 (3–4), 483–496.
Le Roux, L.A., Glendenin, L.E., 1963. Half-life of 232Th. In: Proc. Natl. Meet. Nuclear Energy, Pretoria, South Africa, 83, p. 94.
Leach, D.L., Sangster, D.F., Kelley, K.D., Large, R.R., Garven, G., Allen, C.R., Gutzmer, J., Walters, S., 2005. Sediment-hosted lead-zinc deposits: a global perspective. Econ. Geol. 100 (3), 561–607.
LeHuray, A., Church, S.E., Koski, R.A., Bouse, R., 1988. Pb isotopes in sulfides from mid-ocean ridge hydrothermal sites. Geology 16 (4), 362–365.
Li, Z.X., Mitchell, R.N., Spencer, C.J., Ernst, R., Pisarevsky, S., Kirscher, U., Murphy, J.B., 2019. Decoding Earth's rhythms: Modulation of supercontinent cycles by longer superocean episodes. Precambrian Res. 323, 1–5.
Liew, T., Milisenda, C., Hofmann, A., 1991. Isotopic contrasts, chronology of elemental transfers and high-grade metamorphism: the Sri Lanka Highland granulites, and the Lewisian (Scotland) and Nuk (SW Greenland) gneisses. Geol. Rundsch. 80 (2), 279–288.
Liu, X., Xu, J.-F., Castillo, P.R., Xiao, W., Shi, Y., Zhang, Z., Wang, X.-C., Ao, S., Wang, B., Hu, R., 2021. Long-lived low Th/U Pacific-type isotopic mantle domain: Constraints from Nd and Pb isotopes of the Paleo-Asian Ocean mantle. Earth Planet. Sci. Lett. 567, 117006.
Malaviarachchi, S.P.K., Makishima, A., Tanimoto, M., Kuritani, T., Nakamura, E., 2008. Highly unradiogenic lead isotope ratios from the Horoman peridotite in Japan. Nat. Geosci. 1 (12), 859–863.
Maltese, A., Mezger, K., 2020. The Pb isotope evolution of Bulk Silicate Earth: Constraints from its accretion and early differentiation history. Geochim. Cosmochim. Acta 271, 179–193.
McDonough, W.F., 2007. Mapping the Earth's engine. Science 317 (5842), 1177–1178.
McDonough, W.F., Sun, S.-S., 1995. The composition of the Earth. Chem. Geol. 120, 223–253.
Millot, R., Allègre, C.-J., Gaillardet, J., Roy, S., 2004. Lead isotopic systematics of major river sediments: a new estimate of the Pb isotopic composition of the Upper Continental Crust. Chem. Geol. 203 (1–2), 75–90.
Murakami, T., Chakoumakos, B.C., Ewing, R.C., Lumpkin, G.R., Weber, W.J., 1991. Alpha-decay event damage in zircon. Am. Mineral. 76 (9–10), 1510–1532.
Murphy, D., Kamber, B., Collerson, K., 2003. A refined solution to the first terrestrial Pb-isotope paradox. J. Petrol. 44 (1), 39–53.
Murthy, V.R., Patterson, C., 1962. Primary isochron of zero age for meteorites and the earth. J. Geophys. Res. 67 (3), 1161–1167.
Newsom, H.E., White, W.M., Jochum, K.P., Hofmann, A.W., 1986. Siderophile and chalcophile element abundances in oceanic basalts: Pb isotope evolution and growth of the Earth's core. Earth Planet. Sci. Lett. 80, 299–313.
Niu, Y., 2004. Bulk-rock Major and Trace Element Compositions of Abyssal Peridotites: Implications for Mantle Melting, Melt Extraction and Post-melting Processes beneath Mid-Ocean Ridges. J. Petrol. 45 (12), 2423–2458.
O'neill, H.S.C., 1991. The origin of the Moon and the early history of the Earth—A chemical model. Part 1: The Moon. Geochim. Cosmochim. Acta 55 (4), 1135–1157.
O'Neill, H.S.C., 1991b. The origin of the Moon and the early history of the Earth—A chemical model. Part 2: the Earth. Geochim. Cosmochim. Acta 55 (4), 1159–1172.
Othman, D.B., White, W.M., Patchett, J., 1989. The geochemistry of marine sediments, island arc magma genesis, and crust-mantle recycling. Earth Planet. Sci. Lett. 94 (1–2), 1–21.
Oversby, V., Ringwood, A., 1971. Time of formation of the Earth's core. Nature 234 (5330), 463–465.
Palin, R.M., Santosh, M., Cao, W., Li, S.-S., Hernández-Uribe, D., Parsons, A., 2020. Secular change and the onset of plate tectonics on Earth. Earth Sci. Rev. 207, 103172.
Palin, R.M., White, R.W., 2016. Emergence of blueschists on Earth linked to secular changes in oceanic crust composition. Nat. Geosci. 9 (1), 60–64.
Patterson, C., 1956. Age of meteorites and the earth. Geochim. Cosmochim. Acta 10 (4), 230–237.
Pearson, D.G., Parman, S.W., Nowell, G.M., 2007. A link between large mantle melting events and continent growth seen in osmium isotopes. Nature 449 (7159), 202.
Pearson, D.G., Scott, J.M., Liu, J., Schaeffer, A., Wang, L.H., van Hunen, J., Szilas, K., Chacko, T., Kelemen, P.B., 2021. Deep continental roots and cratons. Nature 596 (7871), 199–210.
Pearson, D.G., Wittig, N., 2008. Formation of Archaean continental lithosphere and its diamonds: the root of the problem. J. Geol. Soc. Lond. 165 (5), 895–914.
Pettke, T., Kodolányi, J., Kamber, B.S., 2018. From ocean to mantle: new evidence for U-cycling with implications for the HIMU source and the secular Pb isotope evolution of Earth's mantle. Lithos 316, 66–76.
Peucker-Ehrenbrink, B., Hofmann, A., Hart, S., 1994. Hydrothermal lead transfer from mantle to continental crust: the role of metalliferous sediments. Earth Planet. Sci. Lett. 125 (1–4), 129–142.
Pineda, C., Schmitt, A.K., Morata, D., 2022. Monazite as a control on Th/U in magmatic zircon. Chem. Geol. 120911.
Plank, T., 2014. The chemical composition of subducting sediments. Elsevier.
Plank, T., Langmuir, C.H., 1998. The chemical composition of subducting sediment and its consequences for the crust and mantle. Chem. Geol. 145 (3–4), 325–394.
Richards, J., 1971. Major lead orebodies, mantle origin? Econ. Geol. 66 (3), 425–434.
Ringwood, A., 1960. Some aspects of the thermal evolution of the earth. Geochim. Cosmochim. Acta 20 (3–4), 241–259.
Ringwood, A.E., Kesson, S.E., Hibberson, W., Ware, N., 1992. Origin of kimberlites and related magmas. Earth Planet. Sci. Lett. 113 (4), 521–538.
Robb, L., 2013. Introduction to ore-forming processes. John Wiley & Sons.
Roden, M., Trull, T., Hart, S., Frey, F., 1994. New he, Nd, Pb, and Sr isotopic constraints on the constitution of the hawaiian plume: results from Koolau Volcano, Oahu, Hawaii, USA. Geochim. Cosmochim. Acta 58 (5), 1431–1440.
Rudge, J.F., Kleine, T., Bourdon, B., 2010. Broad bounds on Earth/'s accretion and core formation constrained by geochemical models. Nat. Geosci. 3 (6), 439–443.
Rudnick, R., Gao, S., Holland, H., Turekian, K., 2003. Composition of the continental crust. The Crust 3, 1–64.
Russell, R., Allan, D., 1955. The age of the earth from lead isotope abundances. Geophys. J. Int. 7, 80–101.
Russell, R.D., Russell, R.D., Farquhar, R.M., 1960. Lead Isotopes in Geology. Interscience Publishers, New York.
Schoenberg, R., Kamber, B.S., Collerson, K.D., Eugster, O., 2002. New W-isotope evidence for rapid terrestrial accretion and very early core formation. Geochim. Cosmochim. Acta 66 (17), 3151–3160.
Schoene, B., 2014. 4.10-u–th–pb geochronology. Treat. Geochem. 4, 341–378.
Shephard, G.E., Matthews, K.J., Hosseini, K., Domeier, M., 2017. On the consistency of seismically imaged lower mantle slabs. Sci. Rep. 7 (1), 1–17.
Shirey, S.B., Richardson, S.H., 2011. Start of the Wilson cycle at 3 Ga shown by diamonds from subcontinental mantle. Science 333 (6041), 434–436.
Spencer, C.J., Kirkland, C.L., Taylor, R.J., 2016. Strategies towards statistically robust interpretations of in situ U-Pb zircon geochronology. Geosci. Front. 7 (4), 581–589.
Sprung, P., Kleine, T., Scherer, E.E., 2013. Isotopic evidence for chondritic Lu/Hf and Sm/Nd of the Moon. Earth Planet. Sci. Lett. 380, 77–87.
Stacey, J.T., Kramers, J., 1975. Approximation of terrestrial lead isotope evolution by a two-stage model. Earth Planet. Sci. Lett. 26 (2), 207–221.
Stanton, R., Russell, R.D., 1959. Anomalous leads and the emplacement of lead sulfide ores. Econ. Geol. 54 (4), 588–607.
Stern, R.J., Gerya, T., Tackley, P.J., 2018. Stagnant lid tectonics: Perspectives from silicate planets, dwarf planets, large moons, and large asteroids. Geosci. Front. 9 (1), 103–119.
Stracke, A., 2021. A process-oriented approach to mantle geochemistry. Chem. Geol. 120350.
Tanaka, R., Nakamura, E., Takahashi, E., 2002. Geochemical evolution of Koolau volcano, Hawaii. Hawaiian Volcanoes 128, 311–332.
Tatsumoto, M., 1966. Genetic relations of oceanic basalts as indicated by lead isotopes. Science 153 (3740), 1094–1101.
Tatsumoto, M., 1978. Isotopic composition of lead in oceanic basalt and its implication to mantle evolution. Earth Planet. Sci. Lett. 38 (1), 63–87.
Tatsumoto, M., Knight, R.J., Allegre, C.J., 1973. Time differences in the formation of meteorites as determined from the ratio of lead-207 to lead-206. Science 180 (4092), 1279–1283.
Tera, F., Wasserburg, G., 1972a. U-Th-Pb systematics in three Apollo 14 basalts and the problem of initial Pb in lunar rocks. Earth Planet. Sci. Lett. 14 (3), 281–304.
Tera, F., Wasserburg, G.J., 1972b. U-Th-Pb systematics in lunar highland samples from the Luna 20 and Apollo 16 missions. Earth Planet. Sci. Lett. 17 (1), 36–51.
Thiemens, M.M., Sprung, P., Fonseca, R.O., Leitzke, F.P., Münker, C., 2019. Early Moon formation inferred from hafnium–tungsten systematics. Nat. Geosci. 12 (9), 696–700.
Van der Hilst, R.D., Widiyantoro, S., Engdahl, E., 1997. Evidence for deep mantle circulation from global tomography. Nature 386 (6625), 578–584.
Van Kranendonk, M.J., Hugh Smithies, R., Hickman, A.H., Champion, D., 2007. secular tectonic evolution of Archean continental crust: interplay between horizontal and vertical processes in the formation of the Pilbara Craton, Australia. Terra Nova 19 (1), 1–38.
Verati, C., Lancelot, J., Hékinian, R., 1999. Pb isotope study of black-smokers and basalts from Pito Seamount site (Easter microplate). Chem. Geol. 155 (1–2), 45–63.
Vollmer, R., 1977. Terrestrial lead isotopic evolution and formation time of the Earth's core. Nature 270 (5633), 144–147.
Wang, W., Cawood, P.A., Spencer, C.J., Pandit, M.K., Zhao, J.-H., Xia, X.-P., Zheng, J.-P., Lu, G.-M., 2022. Global-scale emergence of continental crust during the Mesoarchean–early Neoarchean. Geology 50 (2), 184–188.
Wang, X.-C., Li, Z.-X., Li, X.-H., Li, J., Xu, Y.-G., Li, X.-H., 2013. Identification of an ancient mantle reservoir and young recycled materials in the source region of a young mantle plume: Implications for potential linkages between plume and plate tectonics. Earth Planet. Sci. Lett. 377–378, 248–259.
White, W.M., 1985. Sources of oceanic basalts: Radiogenic isotopic evidence. Geology 13 (2), 115–118.

Wilkinson, J., 2013. Sediment-Hosted Zinc-Lead Mineralization: Processes and Perspectives: Processes and Perspectives.
Willbold, M., Stracke, A., 2010. Formation of enriched mantle components by recycling of upper and lower continental crust. Chem. Geol. 276 (3–4), 188–197.
Williams, I.S., 1997. U-Th-Pb geochronology by ion microprobe.
Wipperfurth, S.A., Guo, M., Šrámek, O., McDonough, W.F., 2018. Earth's chondritic Th/U: Negligible fractionation during accretion, core formation, and crust–mantle differentiation. Earth Planet. Sci. Lett. 498, 196–202.
Wood, B.J., Halliday, A.N., 2010. The lead isotopic age of the Earth can be explained by core formation alone. Nature 465 (7299), 767–770.
Xiang, W., Griffin, W.L., Jie, C., Pinyun, H., Xiang, L., 2011. U and Th contents and Th/U ratios of zircon in felsic and mafic magmatic rocks: improved zircon-melt distribution coefficients. Acta Geol. Sin.-Engl. Ed. 85 (1), 164–174.
Yang, A.Y., Langmuir, C.H., Cai, Y., Michael, P., Goldstein, S.L., Chen, Z., 2021. A subduction influence on ocean ridge basalts outside the Pacific subduction shield. Nat. Commun. 12 (1), 1–10.
Yin, Q., Jacobsen, S., Yamashita, K., Blichert-Toft, J., Télouk, P., Albarede, F., 2002. A short timescale for terrestrial planet formation from Hf–W chronometry of meteorites. Nature 418 (6901), 949–952.
Zartman, R.E., Doe, B.R., 1981. Plumbotectonics—the model. Tectonophysics 75 (1), 135–162.
Zartman, R.E., Haines, S.M., 1988. The plumbotectonic model for Pb isotopic systematics among major terrestrial reservoirs—A case for bi-directional transport. Geochim. Cosmochim. Acta 52 (6), 1327–1339.
Zartman, R.E., Richardson, S.H., 2005. Evidence from kimberlitic zircon for a decreasing mantle Th/U since the Archean. Chem. Geol. 220 (3–4), 263–283.
Zhang, J.-B., Liu, Y.-S., Ducea, M.N., Xu, R., 2020. Archean, highly unradiogenic lead in shallow cratonic mantle. Geology 48 (6), 584–588.
Zhong, S., Zhang, N., Li, Z.-X., Roberts, J.H., 2007. Supercontinent cycles, true polar wander, and very long-wavelength mantle convection. Earth Planet. Sci. Lett. 261 (3–4), 551–564.
Zindler, A., Hart, S., 1986. Chemical geodynamics. Annu. Rev. Earth Planet. Sci. 14, 493–571.